AN ABSTRACT OF THE THESIS OF

James R. Geiselman for the degree of

Master of Science in Agricultural Engineering

presented on July 26, 1984.

Title: Heat Transfer Predictions for

Aquaculture Facilities

Abstract Approved: Redacted for Privacy

Marshall J. English

Recycling of water in aquaculture facilities is used to minimize the amount of energy or tempered water required to control water temperatures. The rate of heat exchange between the water and the environment can be an important variable in the design, management, and economic analysis of a recycle system. A review of heat transfer relationships is presented in this thesis. Combined use of these relationships for predicting the rate of heat transfer from the water in an aquaculture facility is also presented. A comprehensive model is developed from the heat transfer relationships to simulate the primary locations of heat exchange in a salmon production facility. These locations are identified as the air-water interfaces, the soil-wall-water interfaces, the air-wall-water interfaces, the pipes and the aeration processes. The transfer rates are based on the climatic data and physical parameters of the facility.

The model is used to compare predicted and measured rates of heat exchange for a heated water raceway at the Oregon Aqua-Foods

Facility in Springfield, Oregon. The model is also used with a hypothetical raceway and recycle system to determine the relative importance of the different locations of heat exchange and to simulate operational heating costs for relative economic ranking of different operating conditions and design strategies. A comparison is made between predictions based on three-hour data and average daily data. The sensitivity of the predicted net heat transfer rates to the flowrate, soil and wall thermal conductivities, and the thermal convection coefficient between the water and wall is also investigated.

The comparison of the predicted and measured rates of heat transfer indicates that close estimates of the net heat exchange from a raceway can be predicted by the model. Comparisons of daily heat exchange predictions from the three-hour and average daily data showed that the daily data are adequate for estimates, but that three-hour data should be used when more precise estimates are needed (i.e. for sizing heating units). The predicted net heat transfer rates were not significantly affected by the changes in the flowrate, soil and wall thermal conductivities, and the water-to-wall thermal convection coefficient. The air-water interface was found to be the primary location of heat exchange for the specific conditions analyzed and it was concluded that order of magnitude estimates of net heat exchange could be obtained by analyzing the air-water interface and neglecting all other locations. The simulated operational heating costs for the hypothetical system showed a high dependence on ambient and culture water temperatures, and the degree of recycling. Covering open water surfaces during cold

temperature months showed a substantial reduction in the heating costs. Economic simulations demonstrated the value of the model for comparing the relative economics of alternative production strategies.

Heat Transfer Predictions for Aquaculture Facilities

by

James R. Geiselman

A THESIS

submitted to

Oregon State University

in partial fulfillment of
the requirements for the
degree of

Master of Science

Completed July 26, 1984

Commencement June, 1985

APPROVED:

Redacted for Privacy

Associate Professor of Agricultural Engineering
in charge of major

Redacted for Privacy

Head of Department of Agricultural Engineering

Redacted for Privacy

Dean of Graduate School

Date thesis is presented July 26, 1984

Typed by James R. Geiselman

ACKNOWLEDGEMENT

I would like to extend my appreciation and thanks to the many people who have contributed to the development of this thesis.

I am especially grateful for the time and energy given to this project by Marshall J. English, my major professor. His professional insights, patient guidance, and experienced editing contributions were invaluable.

Special recognition is due to associate professor Edward R. Kolbe for his time and knowledge given to numerous questions on heat transfer and aquaculture.

Also, I would like to express my appreciation to professor Carl E. Bond for his valuable insights and comments regarding salmon production.

Special thanks goes to the faculty, staff, and fellow graduate students in the Agricultural Engineering Department at OSU. Their friendly help contributed in many ways to the completion of this thesis. I am especially thankful to E. Stuart Baker for the many hours he spent sharing his expert knowledge of computer software. Recognition is also due to Doug Ernst whose questions, brain storming sessions, and modeling experience helped to make this a more interesting and enjoyable project.

Finally, and most importantly, I would like to thank and acknowledge my wife, Katherine Beale, for her emotional and moral support, her professional editing suggestions, and the many lonely nights and weekends she endured when I was busy with this thesis.

TABLE OF CONTENTS

LIST OF FIGURES

LIST OF TABLES

Heat Transfer Predictions for Aquaculture Facilities

CHAPTER 1

INTRODUCTION

Hatcheries and other types of aquaculture facilities are increasingly turning to temperature control as a management tool for controlling growth rates and minimizing temperature stress to increase the economic viability of their operations. Further economic advantage may be realized if the required heating or chilling is accompanied by a certain level of water treatment and recycling for conservation of water and energy inputs. The water used by these aquaculture facilities will lose or gain a certain amount of heat in the pipes or canals that carry water to the facility, in the culture unit (i.e. the raceway or pond in which the fish are held), and throughout the water treatment and recycle system. The quantity of heat that is exchanged with the environment may be the most important variable in the design, management, and economic analysis of a facility. A model for predicting the heat exchange with a given environment would therefore be of value. More specifically, predictions of heat transfer rates could be used to determine:

1) The monthly and annual heating and chilling energy requirements;
2) The required size of the temperature control units;
3) The quantities of warm or cold water required to maintain a desired water temperature regime in relation to different recycling rates and design strategies for water re-use systems;
4) The locations, quantities, and types of heat losses or gains for analyzing alternative design strategies for energy conservation;
5) The water temperatures throughout the system which affect the

biological, chemical, and physical rates of reaction.

A review of the literature on heat transfer models revealed no documented application of heat transfer relationships for predicting heat exchange rates or water temperatures within aquaculture or water treatment facililties. However, several empirical, semi-empirical, and deterministic relationships have been developed for estimating different components of the overall heat exhange. These components include the evaporative, conductive, longwave and short-wave radiation heat exchanges at air-water interfaces, as well as the conductive and convective transfers to the soil and air at solid interfaces (pipes, raceways, etc.).

This thesis is a documentation of heat transfer relationships and their combined use for predicting the heat exchange between the water and the environment of an aquaculture facility. The specific objectives of the thesis are to:

1) Develop a comprehensive heat transfer prediction model for an aquaculture facility;

2) Validate the model by comparing predicted heat exchange and actual heat exchange for a culture unit (raceway);

3) Evaluate the computation time required by the model by comparing the heat transfer predictions for a culture unit using average 3-hour climatic data and using average 24-hour climatic data;

4) Present an application of the comprehensive model by applying it to a hypothetical recycle facility to predict the total annual, total monthly, and extreme condition heating requirements.

The developement of the comprehensive heat transfer model is divided into five major elements of heat exchange found within a

system:

1) Heat exchange at the air-water interfaces (Chapter 2);

2) Heat exchange to the soil (Chapter 3);

3) Heat exchange to the air through walls (Chapter 4);

4) Heat exchange from pipes (Chapter 5);

5) Heat exchange through aeration processes (Chapter 6).

The theoretical and empirical relationships presented in this development are given in the international system of units. Heat losses from the water are negative and heat gains are positive. The parameters required by the model include dimensions and operating characteristics of the facility, the thermal properties of materials, and regional climatic data consisting of temperatures (dry bulb, wet bulb, and soil), barometric pressure, wind speed, cloud cover, and solar radiation.

The rate of heat transfer between the culture water and the environment is predicted for a heated-water raceway at the Oregon Aqua-Foods fish hatchery in Springfield, Oregon. This predicted value is compared to the observed change in heat content of the water as it passes through the raceway, as determined from the change in water temperature. Two cases of heat transfer were observed for the comparison; One case of net heat loss and one case of net heat gain. The water, air, and wet bulb temperatures, barometric pressure, wind speed, water flowrate, and system dimensions were measured at the site. Solar radiation values were obtained from the University of Oregon Solar Laboratory in Eugene, Oregon. Cloud cover fraction readings were taken from observations at the National Weather Service Station in Eugene, Oregon. Soil

temperatures were determined from values recorded at the Hyslop Farm Experiment Station, Oregon State University, Corvallis, Oregon.

Heat transfer predictions for a hypothetical raceway are determined using a three-hour time step in the analysis and three-hour averages of climatic data. These 3-hour predictions of heat transfer are then compared to the heat transfer predicted using average 24-hour climatic data. Two cases are observed for the comparison; one 24-hour period of warm weather data and one 24-hour period of cold weather data. The climatic data were obtained from observations recorded at the National Weather Service Station, Eugene, Oregon and at the Hyslop Farm Experiment Station, Corvallis Oregon. The sensitivity of the 24-hour predicted net heat transfer rates to the flowrate, the soil and wall thermal conductivities, and the thermal convection coefficient between the water and wall are also investigated for the hypothetical raceway.

A hypothetical recycle aquaculture system is formulated consisting of a culture unit, sedimentation basin, biological filter, areation basin, heat exchanger, and pipe network. Heat transfer predictions for the system are determined for a seven month production schedule of coho salmon fingerlings based on average daily climatic data. Monthly and net production year heat requirements are determined from daily calculations and heating costs are determined for relative economic ranking of different operating conditions and design strategies. The climatic data were taken from observations at the National Weather Service Station, Salem, Oregon and the Hyslop Farm Experiment Station, Corvallis, Oregon.

The results of the heat prediction applications and comparisons

are presented in chapter 7 along with a summary of the assumptions made in the application of the model. Additional research is needed before any statistical inferences can be made concerning the uncertainties inherent in this model. Although these uncertainties may prevent the determination of specific heat quantities with high confidence, it appears that at a minimum the model will yield results that are accurate within an order of magnitude. These results may be used for a better understanding of the heat exchanges taking place in an aquaculture system and for relative rankings of alternative design strategies. A summary of the results and conclusions is presented in Chapter 8.

CHAPTER 2

HEAT TRANSFER AT THE AIR-WATER INTERFACE

2.1 Introduction

The exchange of heat across the air-water interface can be divided into several transfer components which when summed together will give the overall rate of heat transfer. This exchange of heat occurs as a result of radiation, evaporation and conduction. A heat budget for the water surface gives:

$$QAWAT = (HS+HA+HB+HE+HC) \cdot AWAT \qquad 2\text{-}1$$

where

QAWAT = heat transfer rate at the air-water interface (J/s)

HS = shortwave radiation (solar) ($J/m^2/s$)

HA = longwave atmospheric radiation ($J/m^2/s$)

HB = longwave back radiation from the water surface ($J/m^2/s$)

HE = evaporative heat flux ($J/m^2/s$)

HC = conductive heat flux ($J/m^2/s$)

AWAT = area of the air-water interface (m^2)

Typical values for the mean daily transfer rates per unit area are as follows (Thibodeaux, 1979):

HS = 50 to 370 ($J/m^2/s$)

HA = 320 to 420 ($J/m^2/s$)

HB = -320 to -470 ($J/m^2/s$)

HE = 260 to 1050 ($J/m^2/s$)

HC = -40 to +50 ($J/m^2/s$)

Two heat fluxes that are not considered in the heat budget analysis are the fluxes due to the heat contained in the evaporated water,

and in direct rainfall, since these are insignificant in comparison to the other heat fluxes (Ryan and Harleman, 1973).

2.2 Shortwave (Solar) Radiation

The shortwave radiation at the earth's outer atmosphere is dependent on the geographic location, the time of year and the time of day. In passing through the earth's atmosphere it is depleted through absorption and scattering by ozone, dry air, suspended particulate matter and water vapor (Edinger et al.,1973). Upon reaching a horizontal water surface a portion is reflected. The rate of solar energy entering the water surface, HS, is given by (Heinz et al.,1981):

$$HS = HI(1-REFLEC) \qquad 2\text{-}2$$

where

HI = incident solar radiation on the water surface ($J/m^2/s$)

REFLEC = reflectivity of the water surface (0 to 1.)

The incident solar radiation, HI, is most accurately measured by a pyrheliometer. However, stations recording cloud cover are more numerous than those recording ground level radiation (Thibodueax,1979). If pyrheliometer data are not available then average daily values of HI may be calculated from cloud cover readings by an empirical relationship given by Gates (1965):

$$DR = SRA\ (.803 - .340\ CF - .458\ CF^2) \qquad 2\text{-}3$$

where

DR = daily solar radiation on a horizontal surface ($J/m^2/day$)

SRA = daily solar radiation at the top of the atmosphere (extraterrestrial radiation) ($J/m^2/day$)

CF = cloud cover fraction (tenths of sky covered by clouds, 0 to 1.)

Values of SRA have been recorded for a large number of locations or they may be determined for a specific latitude and time of year.

Values of HI for time increments of less than one day may be approximated from DR by modeling the daily radiation as a sine function (see Appendix B, Modeling Solar Radiation As A Sine Function).

The reflectivity of solar radiation at a water surface, REFLEC, has been shown to vary from .04 to .2 over a single day due to the variable angle the sun's rays make with the horizontal water surface. When time increments of one day or greater are being used in the analysis, Ryan and Harleman (1973) advise using average values of reflectivity as given by the USGS Lake Hefner Study (Table 2-1). However, the variation of the reflectivity is too large to be approximated accurately by typical or average values when time increments of less than one day are used (Heinz et al.,1981). The solar reflectivity is a function of the sun's altitude and the type and amount of cloud cover. It can be obtained from an equation given by Anderson (1954):

$$\text{REFLEC} = \text{AC}\left(\frac{180}{\pi}\text{SUN}\right)^{\text{BC}} \qquad 2\text{-}4$$

where

SUN = sun's altitude angle (the angle of the sun above the horizon) (radians)

and AC and BC are constants based upon cloud conditions. Bradey et al.(1969) developed empirical formulas for AC and BC from data taken at the USGS Lake Hefner studies as:

$$\text{AC} = 2.2 + \frac{\text{CR}^{0.7}}{0.4} - \frac{(\text{CR}^{0.7}-0.4)^2}{0.16} \qquad 2\text{-}5$$

$$\text{BC} = -1.2 + \frac{\text{CR}^{0.7}}{0.16} - \frac{(\text{CR}^{0.7}-0.4)^2}{0.64} \qquad 2\text{-}6$$

where

Table 2-1. Suggested daily values of water surface reflectivity, REFLEC, for shortwave radiation (Ryan and Harleman, 1973).

Month	REFLEC
January	0.09
February	0.07
March	0.07
April	0.06
May	0.06
June	0.06
July	0.06
August	0.06
September	0.07
October	0.07
November	0.09
December	0.10

CR = cloudiness ratio

$$= 1. - \frac{HI}{HIMAX} \qquad 2\text{-}7$$

and

HI = incident solar radiation on the water surface ($J/m^2/s$)

HIMAX = maximum clear sky solar radiation ($J/m^2/s$)

The sun's altitude angle, SUN, is derived by analytical geometry (Figure 2-1 and Figure 2-2):

$$\sin(SUN) = \sin(SUN)\sin(D1)+\cos(LAT)\cos(D1)\cos(HANG) \qquad 2\text{-}8$$

where

LAT = geographic latitude (radians)

D1 = declination of the sun (the angle between the line connecting the center of the earth and the sun, and the projection of that line on the equatorial plane) (radians)

$$= \frac{\pi 23.45}{180} \cos\left[\frac{2\pi}{365}(172-DAY)\right] \qquad 2\text{-}9$$

HANG = hour angle of the sun (the angle between the line connecting the center of the earth and the point of interest projected on the equatorial plane, and the projection on that plane of a line from the sun to the center of the earth) (radians)

$$= \frac{\pi}{12}(T - \frac{N}{2} - TRISE) \qquad 2\text{-}10$$

and

DAY = day of the year (Julian date)

T = time of the day (hr)

N = total daylight hours on the day of analysis (hr)

TRISE = time of sunrise (hr)

The average value of the sun's altitude angle during a change in hour angle of H1 to H2 is determined from the average value of the cosine of HANG for the hour angle time increment. The average value of cos(HANG) for the time increment is given by:

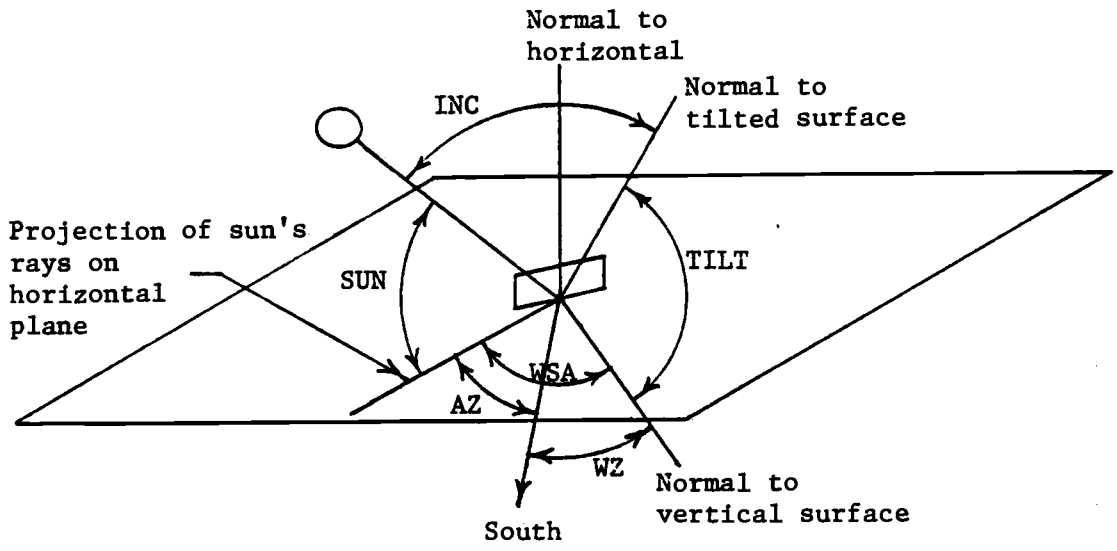

Figure 2-1. Solar angles for an arbitrary tilted surface.

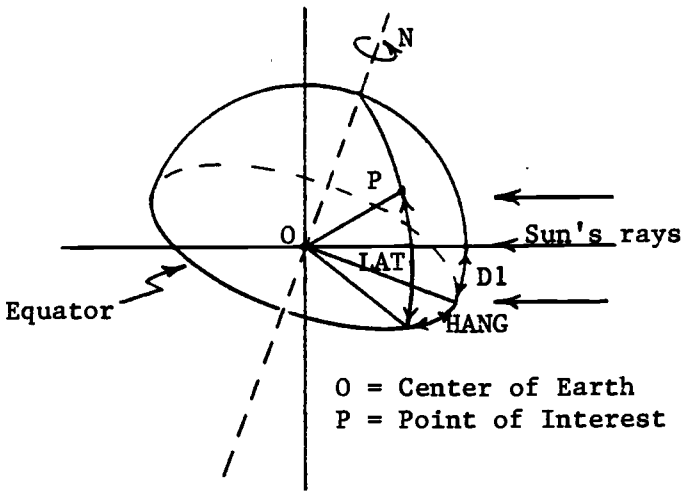

Figure 2-2. Latitude (LAT), hour angle (HANG), and the sun's declination (D1).

$$ACHANG = \frac{\sin(H2)-\sin(H1)}{H2 - H1} \qquad 2\text{-}11$$

where

ACHANG = the average value of the cosine of HANG for the time step of analysis

H1 = hour angle of the sun at time T minus the time step of analysis (radians)

H2 = hour angle of the sun at time T (radians)

The value of the maximum clear sky radiation, HIMAX, can be estimated by (Paily et al.,1974):

$$HIMAX = 0.99\ HIA\cdot(A1+ 0.5(1.-A2)) \qquad 2\text{-}12$$

where

HIA = solar radiation incident to the outer atmosphere ($J/m^2/s$)

$$= \frac{1395.6\ \sin(SUN)}{RATIO^2} \qquad 2\text{-}13$$

RATIO = ratio of the actual to the mean distance from the sun to the earth

$$= 1. + 0.17\ \cos\left[\frac{2\pi}{365}(18.6-DAY)\right] \qquad 2\text{-}14$$

$$A1 = \exp[-MOPT(0.465+0.130MC)(0.179+0.421\cdot\exp(-0.721MOPT)] \qquad 2\text{-}15$$

$$A2 = \exp[-MPOT(0.465+0.134MC)(0.129+0.171\cdot\exp(-0.88MOPT)] \qquad 2\text{-}16$$

and

MOPT = optical air mass

$$= \frac{PRATIO}{\sin(SUN)+0.15\left(\frac{180}{\pi}SUN+3.885\right)^{-1.253}} \qquad 2\text{-}17$$

PRATIO = ratio of air pressure at location altitude to sea level air pressure

$$= \left(\frac{288-0.0065ALT}{288}\right)^{5.256} \qquad 2\text{-}18$$

ALT = altitude in meters

MC = atmospheric moisture content (cm)

$$= 0.85\ \exp(0.110 + 0.0614\ TD) \qquad 2\text{-}19$$

TD = dewpoint temperature (C)

The dewpoint temperature, TD, can be measured or it may be calculated directly from the following equation (ASHRAE,1981):

$$TD = -35.957-1.8726\ell n(100EA)+1.1689[\ell n(100EA)]^2 \qquad 2\text{-}20$$

where

EA = vapor pressure of air (mb) (see Section 2.5)

For any time increment of analysis the values of the average incident solar radiation, HI, and the reflectivity, REFLEC, can be predicted and the resulting net rate of solar radiation, HS, can be calculated. Obstructions to solar radiation such as buildings or trees may be accounted for by identification of the solar azimuth and solar altitude angles of the obstruction (see Appendix C, Solar Obstruction).

2.3 Longwave Atmospheric Radiation

The longwave atmospheric radiation, in contrast to the solar radiation, is more conveniently calculated than measured (Edinger et al.,1974). It is primarily due to the heat content of water vapor, carbon dioxide and ozone components of the atmosphere. Due to variations in the emittance of these three gases an analytic description is not feasible and the longwave radiation is therefore based on empirical relationships (Ryan and Harleman,1973). These relationships have been developed for clear sky radiation and then modified for the effects of clouds.

An equation for clear sky atmospheric radiation developed by Idso and Jackson (1969) gives accurate results for air temperatures above and below the freezing point (Heinz et al.,1981). The equation is:

$$HAC = SB \cdot EMIS\ (TA+273.15)^4 \qquad 2\text{-}21$$

where

HAC = clear sky atmospheric radiation ($J/m^2/s$)

SB = Stefan-Boltzmann constant

$= 5.67 \times 10^{-8} (J/m^2/s/K^4)$

EMIS = clear sky emissivity

$= 1.-0.261 \exp(-.74 \times 10^{-4}\ TA^2)$ 2-22

TA = air temperature (C)

The adjustment for the effect of clouds on the longwave atmospheric radiation is given by the Bolz formula:

$$HAI = HAC\ (1.+ KC \cdot CF^2) \qquad 2\text{-}23$$

where

HAI = incident longwave atmospheric radiation at ground level ($J/m^2/s$)

KC = coefficient dependent on cloud height

CF = cloud cover fraction (0 to 1.)

The value of KC ranges from .04 for cirrus clouds to .25 for nimbostratus or fog (Ryan and Harleman, 1973. A study by the Tennessee Valley Authority (1968) suggests using an average value of .17 for KC (Heinz et al., 1981) which is the value used in the following analysis (Chapter 7).

A final adjustment to account for reflectance at the water surface must be made to the incident longwave atmospheric radiation, HAI. Three percent is usually accepted as the longwave reflectivity at the water surface (Ryan and Harleman, 1973). The net longwave radiation from the atmosphere to the water is therefore:

$$HA = .97\ HAI \qquad (J/m^2/s) \qquad 2\text{-}24$$

2.4 Longwave Radiation From The Water Surface

The longwave radiation from a water surface can be obtained fairly accurately due to precise limits on the emissivity (Ryan and Harleman,1973). According to Anderson (1954) the emmissivity is independent of the water surface temperature and the salt or colloidal concentrations. The emissivity is usually given as 0.97. The longwave (back) radiation, HB, is therefore:

$$HB = -0.97\ SB\ (TW+273.15)^4 \qquad (J/m^2/s) \qquad 2\text{-}25$$

where

SB = Stefan-Boltzmann constant

$= 5.67 \times 10^{-8}\ (J/m^2/s/K^4)$

TW = water temperature (C)

2.5 Evaporative Heat Transfer

Evaporation from a water surface occurs as a result of both forced (wind) and free (buoyant) convection (Ryan and Harleman, 1973). The rate of air movement across the water surface greatly influences the evaporative transfer rate. The primary driving force for evaporation is the difference between the water vapor pressure in the surrounding air and the vapor pressure of the thin layer of air at the water surface (Jirka et al.,1975). Several empirical formulas have been developed for the evaporative heat transfer, HE, based on mass-transfer or turbulent diffusion theory (Paily et al.,1974). The general form of the formulae is:

$$HE = CV \cdot ROW \cdot XLAT \cdot WFUNCZ(EAZ-ESW) \qquad (J/m^2/s) \qquad 2\text{-}26$$

where

CV = conversion factor

= 0.11574 (cm^2.day/m^2/s)

ROW = density of water (g/cm^3)

= 0.999 (g/cm^3) at 15 degrees centigrade

XLAT = latent heat of vaporization (J/g)

WFUNCZ = wind function for height z above the water (cm/day/mb)

EAZ = vapor pressure of air at height z above the water surface (mb)

ESW = saturated vapor pressure at the water surface temperature (mb)

The latent heat of vaporization, XLAT, is given by (Heinz et al., 1981):

$$XLAT = 2500.82 - 2.358\ TW \qquad (J/g) \qquad 2\text{-}27$$

where

TW = water temperature (C)

Several different empirical relationships have been developed for the wind function, WFUNCZ. Gulliver (1977) in work at the University of Minnesota found Ryan and Harleman's (1973) adaptation of Shulyakouskiy's (1969) relationship the most adequate for narrow open channels and small pools (conditions similar to aquaculture facilities). The relationship is for the wind function at a height of 2 meters:

$$WFUNC2 = B2 \cdot WIND + C2 \cdot VIRT^{(1/3)} \qquad 2\text{-}28$$

where

WFUNC2 = wind function for 2 meters above the water (cm/day/mb)

WIND = wind speed 2 meters above the water (m/s)

VIRT = virtual temperature difference between air at the water surface and at 2 meters above the surface (C)

Gulliver (1977) derived best fit values for the constants B2 and C2 as:

B2 = .00832

C2 = .00960

The virtual temperature is defined as the temperature which dry air would have if its pressure and density were the same as the given sample of moist air. The relationship for the virtual temperature difference, VIRT, is:

$$VIRT = TW\left(1.+\frac{0.378ESW}{PA}\right) - TA2\left(1.+\frac{0.378EA2}{PA}\right) \qquad 2\text{-}29$$

where

TW = water temperature (C)

TA2 = air temperature at a height of 2 meters above the water surface (C)

ESW = saturated vapor pressure at the water temperature (mb)

EA2 = vapor pressure at a height of 2 meters above the water surface (mb)

In general, the vapor pressure of air, EA, can be determined from either the relative humidity, RH (percent), and saturation vapor pressure, ESA, by:

$$EA = ESA \frac{RH}{100} \qquad 2\text{-}30$$

or from the wet bulb and dry bulb temperatures (Campbell,1977):

$$EA = ESWB - \frac{PA \cdot SPHA(TA-TWB)}{622\ XLAT} \qquad 2\text{-}31$$

where

EA = vapor pressure at air temperature TA (mb)

ESA = saturated vapor pressure at air temperature TA (mb)

ESWB = saturated vapor pressure at wet bulb temperature TWB (mb)

PA = atmospheric pressure (mb)

SPHA = specific heat of dry air (1006. J/Kg/C)

TA = air temperature (C)

TWB = wet bulb temperature (C)

XLAT = latent heat of vaporization (J/g)

The value of EA2 is the vapor pressure EA determined by either the relative humidity or the air and wet bulb temperatures at a height of 2 meters above the water surface. The value of XLAT can be determined from equation 2-27 given by Heinz using TWB in place of TW since the relationship for EA is based on the evaporation of water at the wet bulb temperature. The saturated vapor pressures, ESW, ESA and ESWB can be computed from the Magnus-Teton's formula (Murray,1976):

$$ES = 6.1078 \exp\left(\frac{17.26939TEM}{TEM+237.29}\right) \qquad 2\text{-}32$$

where

ES = saturated vapor pressure (mb)

TEM = temperature of the air-vapor mixture (C)

The rate of evaporative heat transfer, HE, can be predicted from the above relationships. The resulting empirical equation for HE based on the 2 meter wind function WFUNC2 is:

$$HE = CV \cdot ROW \cdot XLAT \cdot WFUNC2(EA2-ESW) \qquad 2\text{-}33$$

The environmental parameters required are the water surface temperature, TW, the air temperature at 2 meters above the water surface,TA2, the wind speed at 2 meters, WIND, the atmospheric pressure, PA, and either the relative humidity, RH, or the wet bulb temperature, TWB, at 2 meters.

2.6 Conductive Heat Transfer

The conductive heat transfer from the water to the air is usually related to the evaporative heat transfer by the Bowen(1926) ratio, BOWEN (Jirka et al.,1975; Heinz et al.,1981). The relationship is:

$$HC = BOWEN \cdot HE \qquad 2\text{-}34$$

where

HC = conductive heat flux at the air-water interface ($J/m^2/s$)

HE = evaporative heat flux ($J/m^2/s$)

and

$$BOWEN = \frac{0.61PA(TW-TA2)}{1000(ESW-EA2)} \qquad 2\text{-}35$$

where all other variables are as given for the evaporative heat transfer. The basis for this relationship is the assumption that the eddy diffusivities for heat and mass (vapor) are equal (Jirka et al.,1975).

In cases where the evaporative heat loss is less than or equal to zero, the conductive heat transfer may be calculated by a relationship given by Thibodeaux (1979):

$$HC = 1.53\ WIND(TA-TW) \qquad 2\text{-}36$$

where

WIND = wind speed (m/s)

TA = air temperature (C)

TW = water temperature (C)

CHAPTER 3

HEAT TRANSFER TO SOIL

3.1 Introduction

Heat transfer between a raceway or pond and the surrounding soil is a function of several time dependent variables that may be difficult to accurately identify. Among these variables are the soil thermal conductivity and heat capacity which are dependent on the volume fractions of air, water, minerals and organic matter in the soil(VanWijk,1963; Sellers,1965). Non-homogeneous soils will have spatially varying thermal properties. Other variables include the soil temperature, the air temperature and the thermal properties of the material separating the water and the soil (e.i. concrete walls).

Heat transfer to the soil has been neglected as insignificant in all hydro-thermal models encountered in the literature for open bodies of water. Hienz et al.(1981) measured rates of heat transfer to the soil from heated water in open channels and small pools in cold weather conditions (Minnesota winter) and found it to be negligable. A finite difference model was developed in Section 3.2 for a hypothetical sub-grade water containment structure (raceway). Preliminary analysis of the open (uncovered) raceway using the finite difference soil model showed heat transfer to the soil was between one and five percent as great as the air-to-water heat transfer, where the air-to-water heat transfer was approximated by a simplified heat exchange model (Analysis of the hypothetical raceway for a hot and cold day, section 7.3, showed the soil heat transfer to be

less than one percent of the total heat transfer). It was therefore assumed that because of the inaccuracies inherent in the model parameters and the relative insignificance of the quantity of heat exchange to the soil as compared to the heat exchange to the air, a complex model of the soil heat transfer would be of no significant additional value over a simplified approximation model. In addition it was determined that the heat transfer to the soil should be based on a steady-state soil temperature profile determined from regional data of the daily average ambient soil and soil surface temperatures as boundary conditions (Section 3.2). The determination of the steady-state heat transfer rate by the finite difference model is more costly in computer time than is a simplified steady-state model. The finite difference model also requires the identification of the soil heat capacity and additional soil temperatures that are not required by the simplified model. If uniform grid sizes are to be maintained for the finite difference analysis, a new grid system and set of equations is required when different raceway design configurations are analyzed. With the simplified model the same equations can be used with different dimensional parameters. Thus the finite difference model is also less adaptable to design changes than the simplified model. A more general, simplified model was therefore developed in Section 3.3 and compaired to solutions from the finite difference model.

The comparison of the finite difference and simplified models used a wide range of hypothetical combinations of different materials and environmental parameters. This included extreme cases of high thermal conductivities for the soil and containment walls

coupled with large temperature differences between the water and the soil. The simplified model consistantly predicted a soil heat transfer rate between 60 and 70 percent of the rate predicted by the finite difference model in both cases of heat gain and heat loss. Considering the consistent difference between the prediction values given by the two models it appears that a correction coefficient could be used to correct the simplified prediction value. Additional research is needed in this area to investigate the effect on the relative difference resulting from changes in the buried depth of the raceway. Assuming that the heat transfer to the soil represents less than 5 percent of the total heat transfer with the environment (for open air raceways), the difference between using the simplified model in place of the finite difference model would be less than 2 percent of the total heat transfer with the environment.

3.2 Finite Difference Soil Heat Transfer Model

For heat transfer to the soil from a rectangular containment of water it is assumed that the longitudinal temperature variation is negligible in comparison to the transverse temperature variation. A two dimensional analysis using the transverse horizontal and vertical directions is therefore used in the development of the model. The boundary conditions for the analysis will be set at the soil surface and at a distance of two meters from the containment surfaces. These conditions are respectively, the ambient soil surface temperature and sub-surface temperatures. It is assumed that these ambient boundary conditions are insignificantly affected by heat transfer from the water. A grid system for the analysis can be defined as in Figure 3-1. Boundary conditions are symmetric about the centerline of the raceway which therefore represents an adiabatic plane. The variables for the analysis are defined as:

$T_{i,1}$ = soil temperature at the ith node at time T (C)

$T_{i,2}$ = soil temperature at the ith node at time T plus the time step of analysis (C)

TW = water Temperature (C)

TS = soil surface temperature (C)

WX = width of the containment walls (m)

X = soil cell width for finite difference grid (m)

KW = thermal conductivity of the water containment wall (J/m/s/C)

KS = thermal conductivity of the soil (J/m/s/C)

CS = heat capacity of the soil ($J/m^3/C$)

HCONW = convective heat transfer coefficient between the water and wall ($J/m^2/s/C$) (Appendix D gives empirical relationships for convective heat transfer coefficients)

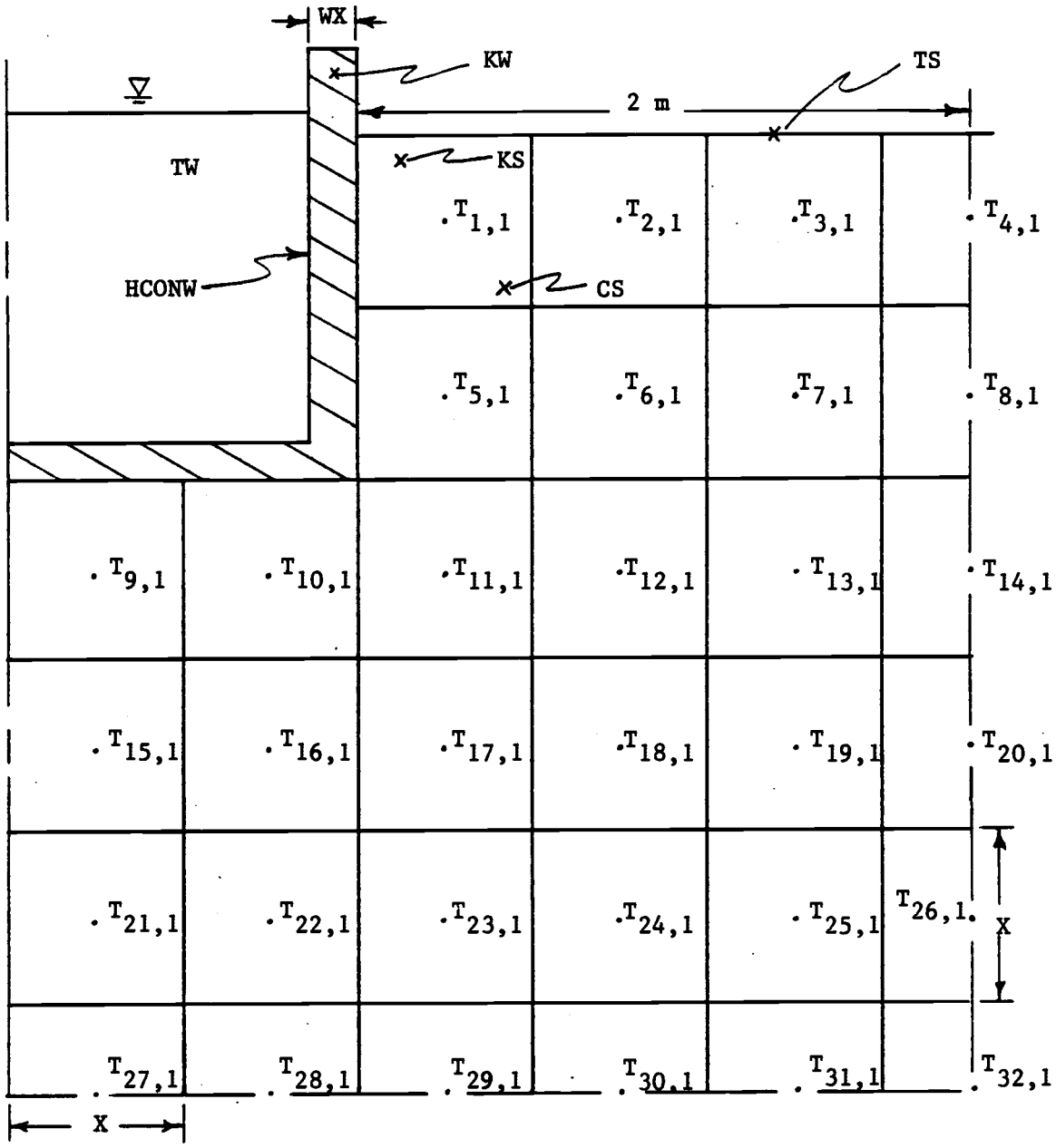

Figure 3-1. Finite difference soil model grid configuration.

STEP = time step of analysis (s)

Fourier's "second law" of heat conduction for one dimensional heat flow in the x direction with constant thermal properties is given by the relationship:

$$\frac{dT\ CS}{dt} = KS\ \frac{d^2T}{dx^2} = KS\ \frac{d}{dx}\left(\frac{dT}{dx}\right) \qquad 3\text{-}1$$

The approximation of this relationship by finite difference analysis for a soil cell having a soil node temperature T_i gives:

$$\frac{(T_{i,2} - T_{i,1})\ CS}{STEP} = \frac{KS}{X^2}\left(T_{i+1,1} + T_{i-1,1} - 2\ T_{i,1}\right) \qquad 3\text{-}2$$

This approximation can be extended to the two dimensional heat transfer analysis. Given the ambient soil temperatures that define the boundary conditions, the following expressions can be derived for predicting the temperatures at the soil temperature nodes for successive time increments.

Let:

$$DM = \frac{STEP \cdot KS}{X^2 \cdot CS} \qquad 3\text{-}3$$

$$HM = \frac{STEP}{X \cdot CS\left(\frac{WX}{KW} + \frac{X}{2KS} + \frac{1}{HCONW}\right)} \qquad 3\text{-}4$$

Then for temperature nodes 11,12,13,16,17,18,19,22,23,24,25

$$T_{i,2} = T_{i,1} + (T_{i+1,1} + T_{i-1,1} + T_{i+6,1} + T_{i-6,1} - 4\ T_{i,1}) \cdot DM \qquad 3\text{-}5$$

and for the remaining temperature nodes

$$T_{1,2} = T_{1,1} + (2 \cdot TW + T_{2,1} + T_{5,1} - 4 \cdot T_{1,1}) \cdot DM + (TW - T_{1,1}) \cdot HM \qquad 3\text{-}6$$

$$T_{2,2} = T_{2,1} + (2 \cdot TW + T_{1,1} + T_{3,1} + T_{6,1} - 5 \cdot T_{2,1}) \cdot DM \qquad 3\text{-}7$$

$$T_{3,2} = T_{3,1} + (2 \cdot TW + T_{2,1} + T_{4,1} + T_{7,1} - 5 \cdot T_{3,1}) \cdot DM \qquad 3\text{-}8$$

$$T_{5,2} = T_{5,1} + (T_{1,1} + T_{6,1} + T_{11,1} - 3 \cdot T_{5,1}) \cdot DM + (TW - T_{5,1}) \cdot HM \qquad 3\text{-}9$$

$$T_{6,2} = T_{6,1} + (T_{2,1} + T_{5,1} + T_{7,1} + T_{12,1} - 4 \cdot T_{6,1}) \cdot DM \qquad 3\text{-}10$$

$$T_{7,2} = T_{7,1} + (T_{3,1} + T_{6,1} + T_{8,1} + T_{13,1} - 4 \cdot T_{7,1}) \cdot DM \quad 3\text{-}11$$

$$T_{9,2} = T_{9,1} + (T_{10,1} + T_{15,1} - 2 \cdot T_{9,1}) \cdot DM + (TW - T_{9,1}) \cdot HM \quad 3\text{-}12$$

$$T_{10,2} = T_{10,1} + (T_{9,1} + T_{11,1} + T_{16,1} - 3 \cdot T_{10,1}) \cdot DM + (TW - T_{10,1}) \cdot HM \quad 3\text{-}13$$

$$T_{15,2} = T_{15,1} + (T_{9,1} + T_{16,1} + T_{21,1} - 3 \cdot T_{15,1}) \cdot DM \quad 3\text{-}14$$

$$T_{21,2} = T_{21,1} + (T_{15,1} + T_{22,1} + T_{27,1} - 3 \cdot T_{21,1}) \cdot DM \quad 3\text{-}15$$

The average net heat transfer rate from the water to the soil, QFIN, for a time step of analysis, is calculated from the soil temperature nodes at the containment structure boundary, 1,5,9,and 10, by:

$$QFIN = \left[(T_{1,1} + T_{1,2} + T_{5,1} + T_{5,2} + T_{9,1} + T_{9,2} + T_{10,1} + T_{10,2})/2 - 4 \cdot TW\right] \cdot SM \quad 3\text{-}16$$

where

$$SM = \frac{WX}{KW} + \frac{X}{2KS} + \frac{1}{HCONW} \quad 3\text{-}17$$

If the total overall coefficient being multiplied by the soil node temperatures $T_{i,1}$ in the above equations is negative then the temperature at $T_{i,2}$ will be reduced as the value of $T_{i,1}$ increases. This would violate thermodynamic principles and it therefore follows that for a given cell width X, the time step of analysis, STEP, must be chosen to give a non-negative value for the total overall coefficient. This is a sufficient condition to insure stability for the solution of explicit finite difference equations (Croft and Lilley,1977). Based on this requirement, analysis of the developed equations for T gives two limiting conditions for STEP to insure stability. The conditions are:

1) $$STEP \leq 1 \Big/ \left(\frac{4KS}{X^2 \cdot CS} + \frac{1}{SM \cdot X \cdot CS} \right) \quad 3\text{-}18$$

and

2) $$STEP \leq \frac{X^2 \cdot CS}{5KS} \quad 3\text{-}19$$

Further analysis shows that if

$$KS/X \leq 1./(WX/KW+X/2./KS+1./HCONW) \qquad 3\text{-}20$$

then condition 1) insures stability or if

$$KS/X > 1./(WX/KW+X/2./KS+1./HCONW) \qquad 3\text{-}21$$

then condition 2) insures stability.

Simulation of soil heat transfer with the finite difference model shows that changes in the soil temperature profile are very slow due to the large heat capacity and small thermal conductivity of most soils. The heat transfer rate at a given hour or day is essentially at steady-state with the existing soil temperatures at the time of analysis and is therefore highly dependent on the specified soil temperature profile. A relationship for the ambient soil temperature as a function of the time and the soil depth, thermal properties and soil surface temperature (Sellers,1965; Carslaw and Jaeger,1959) was initially used for the identification of the soil temperature boundary conditions. The daily fluctuations in the soil temperatures at a distance of two meters from the water containment walls had an insignificant effect on the heat transfer rate when the model was tested. The soil surface temperature is a difficult parameter to predict, being dependent on solar radiation, longwave radiation, sensible and latent heat exchanges (Thibodeaux, 1979). Sellers (1965) reports that daily soil temperature fluctuations penetrate to depths of from .2 to .8 meters. Calculations with the ambient soil temperature-depth relationship showed that significant fluctuations penetrate to much shallower depths.

In reviewing the above findings with respect to the heat transfer to the soil (the dependence on the initial soil temperatures,

the slow changes in the soil temperatures and thus the transfer rate, the insignificance of the daily soil temperature fluctuations, and the difficulty in accurately predicting the soil and soil surface temperatures) the heat transfer to the soil will be based on a steady-state temperature profile determined from regional data for daily average ambient soil and soil surface temperatures as the boundary conditions. This will be the procedure for the development and comparison of the simplified water-to-soil heat transfer model.

3.3 Simplified Soil Heat Transfer Model

The objective of the simplified soil heat transfer model is to derive approximate estimates of the heat transfer rate with less computer time, less specification of variables, and greater adaptibility to different raceway configurations then is possible with the finite difference model.

The simplified heat transfer rate will be based on steady-state soil node temperatures calculated from the average daily soil temperatures and the temperature of the water. The soil boundary conditions are set at two meters from the containment structure walls as in the finite difference analysis. A general two dimensional diagram of the heat transfer process is illustrated in Figure 3-2. The following variables are utilized in the analysis:

TW = water temperature

TO = steady-state soil temperature for the node

T1 = steady-state soil temperature for the node

T2 = steady-state soil temperature for the node

DX = depth of the containment structure below the surface (m)

TSS = average daily soil surface temperature (C)

TSO = average daily soil temperature at a depth of one half DX

TS1 = average daily soil temperature at a depth of DX plus one meter

TB = average daily soil temperature at a depth of DX plus two meters

L = length of the containment structure (m)

WR = inside width of containment structure (m)

WX = material width of the side walls (m)

BX = material width of base (m)

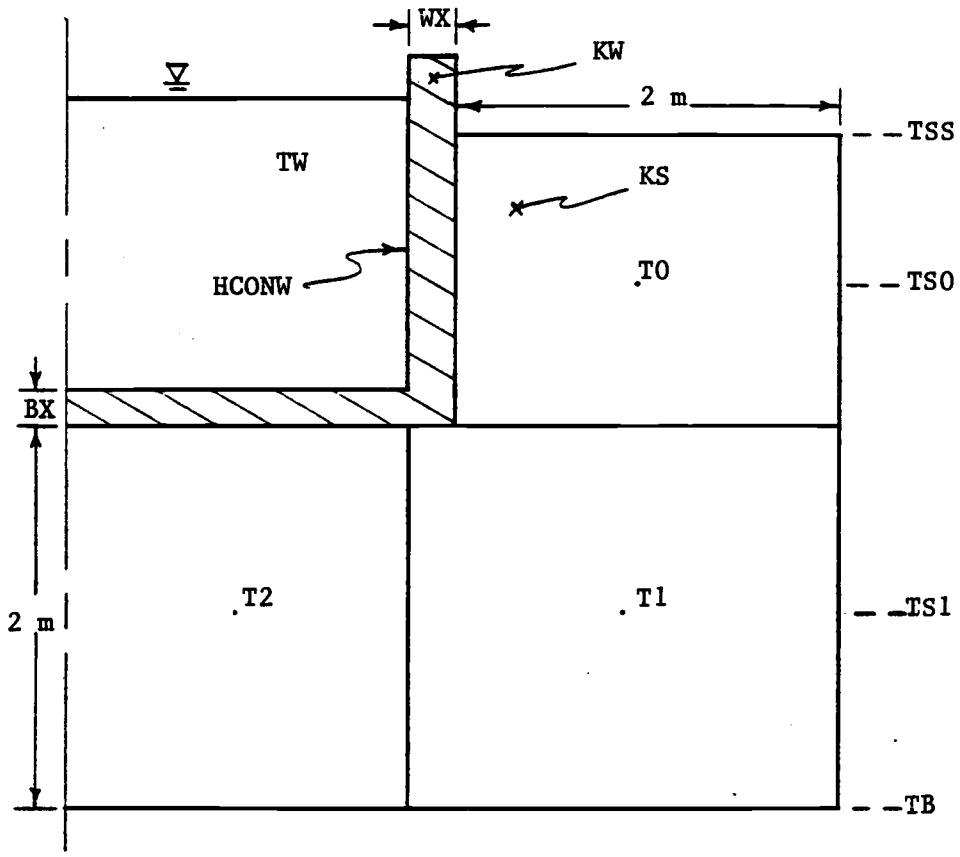

Figure 3-2. Simplified soil model configuration.

KW = thermal conductivity of the water containment structure material (J/m/s/C)

KS = thermal conductivity of the soil (J/m/s/C)

HCONW = convective heat transfer coefficient between the water and the wall ($J/m^2/s/C$) (Appendix E)

From a steady-state heat balance analysis of the three representative soil cells (setting the sum of the heat exchanges at the soil cell boundaries equal to zero) the steady-state temperatures TO, T1 and T2 can be determined. For the soil cell represented by the soil node temperature TO, the analysis gives:

$$0 = \frac{4 \cdot L \cdot KS(TSS-TO)}{DX} + \frac{L \cdot DX(TW-TO)}{\left(\frac{WX}{KW}+\frac{1}{KS}+\frac{1}{HCONW}\right)} + \frac{2 \cdot L \cdot KS(T1-TO)}{1+0.5DX}$$

$$+ L \cdot DX \cdot KS(TSO-TO) \qquad 3\text{-}22$$

For the soil cell represented by the soil node temperature T1:

$$0 = L \cdot KS(TO-T1)+2 \cdot L \cdot KS(TS1-T1) + \frac{2 \cdot L \cdot KS(T2-T1)}{(WX+0.25WR+1)}$$

$$+ 2 \cdot L \cdot KS(TB-T1) \qquad 3\text{-}23$$

For the soil cell represented by the soil node temperature T2:

$$0 = \frac{0.5L \cdot WR(TW-T2)}{\left(\frac{BX}{KW}+\frac{1}{KS}+\frac{1}{HCONW}\right)} + \frac{2 \cdot L \cdot KS(T1-T2)}{(WX+0.25WR+1)} + 0.5L \cdot WR \cdot KS(TB-T2) \qquad 3\text{-}24$$

Let:

$$A = \frac{0.5L \cdot WR}{V1} + \frac{2 \cdot L}{V2} + 0.5L \cdot WR \qquad 3\text{-}25$$

$$B = 2.5+\frac{1}{V2} \qquad 3\text{-}26$$

$$C = \frac{4 \cdot L}{DX}+\frac{L \cdot DX}{V3} + \frac{2 \cdot L}{(1+0.5DX)} + L \cdot DX \qquad 3\text{-}27$$

$$D = \frac{0.5L \cdot WR \cdot TW}{V1} + 0.5L \cdot WR \cdot TB \qquad 3\text{-}28$$

$$E = TS1+TB \qquad 3\text{-}29$$

$$F = \frac{4 \cdot L \cdot TSS}{DX} + \frac{L \cdot DX \cdot TW}{V3} + L \cdot DX \cdot TSO \qquad 3\text{-}30$$

$$G = 2 \cdot L/V2 \qquad 3\text{-}31$$

$$H = 1./V2 \qquad 3\text{-}32$$

$$I = 2 \cdot L/(1.+DX\ .5) \qquad 3\text{-}33$$

$$J = .5 \qquad 3\text{-}34$$

where

$$V1 = \frac{KS \cdot BX}{KW} + 1 + \frac{KS}{HCONW} \qquad 3\text{-}35$$

$$V2 = WX + 0.25WR + 1 \qquad 3\text{-}36$$

$$V3 = \frac{KS \cdot WX}{KW} + 1 + \frac{KS}{HCONW} \qquad 3\text{-}37$$

then

$$T1 = \frac{E \cdot A \cdot C + H \cdot D \cdot C + A \cdot F \cdot J}{B \cdot A \cdot C - G \cdot H \cdot C - A \cdot I \cdot J} \qquad 3\text{-}38$$

$$T2 = \frac{D + G \cdot T1}{A} \qquad 3\text{-}39$$

$$T0 = \frac{F + I \cdot T1}{C} \qquad 3\text{-}40$$

The net heat transfer rate, QSIMP, for the right half of the containment structure shown in Figure 3-2 is calculated from the heat exchange between the water and the steady-state soil temperatures T0 and T2. The relationship is given by:

$$QSIMP = \frac{L \cdot DX \cdot KS(TO-TW)}{V1} + \frac{0.5L \cdot WR \cdot KS(T2-TW)}{V3} \qquad (J/s) \qquad 3\text{-}41$$

CHAPTER 4

HEAT TRANSFER TO THE AIR THROUGH CONTAINMENT SURFACES

4.1 Conduction And Convection

Heat transfer to the air through containment structure walls can be calculated from basic heat transfer theory for conduction and convection as presented by Welty et al.(1976). The rate of heat transfer is dependent on the convective resistances at the air-to-wall and water-to-wall interfaces and the thermal conductivity of the material. The relation is given by:

$$QWAL = AWAL \cdot TCOEF(TA-TW) \qquad 4\text{-}1$$

where

QWAL = the overall heat transfer rate between air and water through the containment structure wall (J/s)

AWAL = area of the air-wall-water interface (m^2)

TCOEF = the overall heat transfer coefficient for the wall

$$= \left(\frac{1}{HCONW} + \frac{WX}{KW} + \frac{1}{HCONA}\right)^{-1} \qquad (J/m^2/s/C) \qquad 4\text{-}2$$

and

HCONW = convective heat transfer coefficient between the water and the wall ($J/m^2/s/C$)

WX = material width of the containment walls (m)

KW = conductivity of the containment walls (J/m/s/C)

HCONA = convective heat transfer coefficent between the air and the wall ($J/m^2/s/C$)

Appendix D gives several empirical relationships for approximating the convective heat transfer coefficients.

4.2 Sunlit Walls

The heat transfer analysis of water containment surfaces that are exposed to direct solar radiation requires application of the "sol-air" temperature concept. The sol-air temperature is the air temperature which, neglecting all radiation effects, would give the same rate of heat exchange as would result from the actual incident solar radiation, longwave radiation and convective transfer with the ambient air (ASHRAE, 1981).

The heat flux into a sunlit surface based on the actual radiation is given by:

$$HFLUX = SAB \cdot HIS + HCR(TA - TSUR) - EMIT \cdot DRAD \qquad (J/m^2/s) \qquad 4\text{-}3$$

where

SAB = solar absorptance of the surface

HIS = incident solar radiation on the surface ($J/m^2/s$)

HCR = coefficient of heat transfer by longwave radiation and convection at the outer surface ($J/m^2/s/C$)

TA = air temperature (C)

TSUR = surface temperature (C)

EMIT = emittance of the surface

DRAD = the difference between the longwave radiation from the sky and surroundings and from a black body at the air temperature ($J/m^2/s$)

The heat flux based on the sol-air temperature, TSOL, is given by:

$$HFLUX = HCR(TSOL - TSUR) \qquad 4\text{-}4$$

From these two equations for the heat flux at the surface of the containment wall, the sol-air temperature is:

$$TSOL = TA + \frac{HIS \cdot SAB}{HCR} - \frac{EMIT \cdot DRAD}{HCR} \qquad 4\text{-}5$$

The sol-air temperature, TSOL, can be used in equation 4-1 in place

of the air temperature, TA, for determining the heat transfer rate for sun lit walls.

For the net longwave radiation difference, DRAD, the ASHRAE Fundamentals Handbook (1981) recommends a value of 63 $J/m^2/s$ for horizontal surfaces receiving longwave radiation from the sky only and a value of zero for vertical surfaces (since the incoming and outgoing radiation are approximatly equal). For the ratio of the absorptance to convective coefficient, SAB/HCR, the ASHRAE handbook gives a value of 0.026 for a light-colored surface and 0.052 for a dark-colored surface. The incident solar radiation on the water containment surface, HIS, must be identified for the time increment of analysis. Section 2.2 gives information for determination of the incident solar radiation on a horizontal plane (water surface) at the surface of the earth, HI. Appendix B describes a method for modeling the daily solar radiation as a sine function for analyzing time increments that are less than one day. Obstructions to the solar radiation such as trees, buildings, or mountains can be accounted for by the identification of the obstruction angles as outlined in Appendix C.

The incident solar radiation at the earth's surface, HI, is equivalent to HIS for horizontal surfaces. For vertical or tilted surfaces however, the value of the incident solar radiation, HIS, must be determined from the solar orientation in relation to the direction of HI. Mcquiston and Parker (1982) relate the normal direct radiation on a horizontal plane, GND, to the incident radiation on a tilted surface, HIS, by the following relationship:

$$HIS = GND \cos(INC) \qquad 4\text{-}6$$

where

INC = the angle of incidence for the surface (the angle between the sun's rays and the normal to the surface, Figure 2-1)

The angle of incidence, INC, is identified by the following analytic geometry relationship:

$$\cos(INC) = \cos(SUN)\cos(WSA)\cos(TILT)+\sin(SUN)\sin(TILT) \quad 4\text{-}7$$

where

SUN = sun's altitude angle (the angle the sun's rays make with a horizontal plane)

WSA = wall solar azmuth angle (the angle measured in the horizontal plane between the projection of the sun's rays and the projection of the normal to the surface)

TILT = angle of tilt for the surface (the angle between the normal to the surface of the wall and the normal to a vertical surface)

The determination of the sun's altitude angle, SUN, was presented earlier (Section 2.2) as a function of the time of day (hour angle, HANG), the day of the year (declination, D1) and the location latitude, LAT. The computation of the wall solar azimuth angle, WSA, is dependent on the following conditions:

a) For afternoon hours with walls facing west of south and morning hours with walls facing east of south:

WSA = absolute value of (AZ-WZ) 4-8

b) For afternoon hours with walls facing east of south and morning hours with walls facing west of south:

WSA = absolute value of (AZ+WZ) 4-9

where

AZ = solar azimuth angle (the angle between south and the projection of the sun's rays on a horizontal plane)

WZ = wall azimuth angle (the angle east or west of south to the normal to the surface projected on the horizontal plane)

The determination of the solar azimuth angle, AZ, is presented in Appendix C as a function of the solar altitude angle.

The value of the normal direct radiation on a horizontal surface, GND, needed for the determination of HIS, can be calculated from values of incident solar radiation on a horizontal surface, HI. For a horizontal surface, HIS equals HI, the cos(INC) equals sin(SUN), and the equation for HIS as a function of GND becomes:

$$HI = GND \sin(SUN) \qquad 4\text{-}10$$

Substitution back into the equation for the incident solar radiation equation for a tilted surface gives:

$$HIS = \frac{HI \cos(INC)}{\sin(SUN)} \qquad 4\text{-}11$$

For vertical surfaces this becomes:

$$HIS = \frac{HI \cos(SUN) \cos(WSA)}{\sin(SUN)} \qquad 4\text{-}12$$

Thus the values of the incident solar radiation on a horizontal surface (water surface), HI, as presented in Section 2.2 can be used to determine the incident solar radiation on a tilted containment surface, HIS, needed for the calculation of the sol-air temperature, TSOL. The sol-air temperature is then used in equation 4-1 in place of the air temperature to determine the overall heat transfer rate, QWAL, between the air and water.

CHAPTER 5

HEAT TRANSFER FROM PIPES

5.1 Heat Transfer From Buried Pipes

Kendrick and Havens (1973) used the method of images (Jakob, 1949) to develop a theoretical relationship for predicting the heat transfer from a pipe buried in a homogeneous soil having a constant soil surface temperature (Figure 5-1). In the analysis the thermal resistance of the pipe is neglected by assuming that the outside surface temperature of the pipe is equal to the temperature of the water. It is also assumed that there is no temperature variation in the radial direction within the pipe. The equation they derive is:

$$QPZ = 2\pi CP(TS-TOR) \qquad 5\text{-}1$$

where

QPZ = lateral heat flowrate per unit length of pipe at longitudinal coordinate z (J/s/m)

$$CP = \frac{KS}{\ln\left(\frac{2DEP-RO}{RO}\right)} \qquad 5\text{-}2$$

KS = thermal conductivity of soil (J/m/s/C)

DEP = depth pipe is buried, measured to the pipe centerline (m)

RO = outside radius of the pipe (m)

TOR = temperature of the pipe surface at the outside radius of the pipe, RO, at longitudinal coordinate z (C)

TS = temperature of the soil surface (C)

To analyze the effects of using different pipe materials, this equation must be adapted to account for the thermal resistance to heat transfer through the pipe. From Welty et al. (1976) the heat flowrate in the radial direction from a pipe (Figure 5-2) is

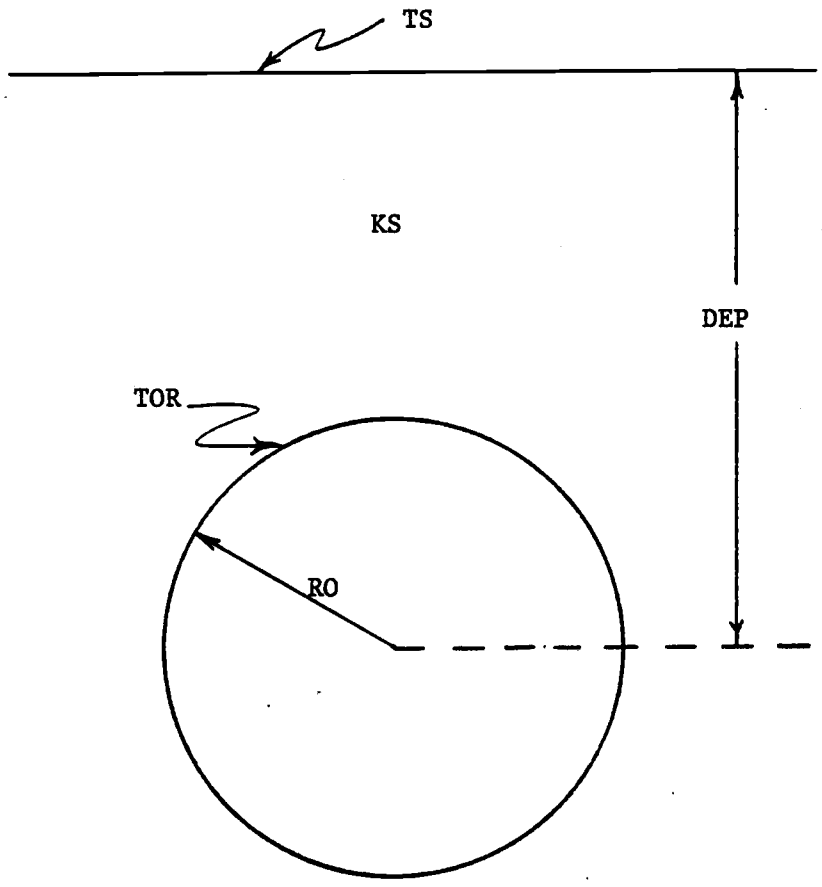

Figure 5-1. Buried pipe diagram for Kendrick and Havens analysis.

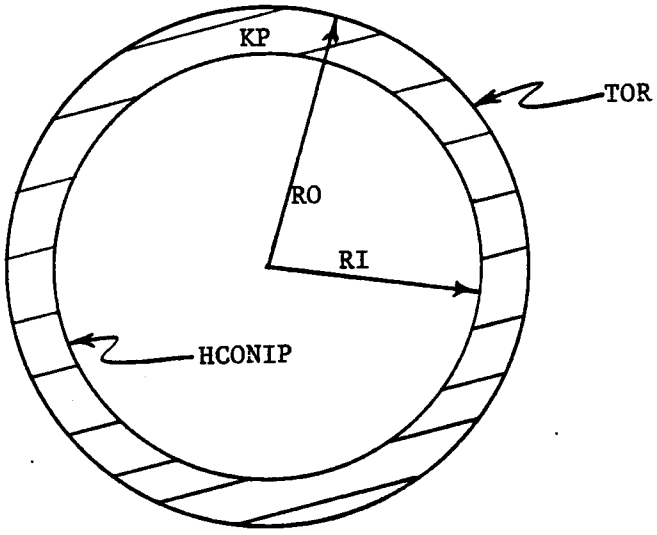

Figure 5-2. Pipe diagram for basic heat transfer analysis.

given by the theoretical relationship:

$$QPZ = 2\pi DP(TOR-TW) \qquad 5\text{-}3$$

where

$$DP = \left(\frac{1}{HCONIP \cdot RI} + \frac{\ell n(RO/RI)}{KP}\right)^{-1} \qquad 5\text{-}4$$

TW = temperature of the water in the pipe at the longitudinal coordinate z (C)

HCONIP = convective heat transfer coefficient for the inside surface of the pipe ($J/m^2/s/C$) (see Appendix D, Convective Heat Transfer Coefficients)

KP = thermal conductivity of the pipe material (J/m/s/C)

RO = outside radius of the pipe (m)

RI = inside radius of the pipe (m)

Setting equation 5-1 equal to equation 5-3 gives:

$$(TS-TOR)CP = (TOR-TW)DP \qquad 5\text{-}5$$

and

$$TOR = (TS\ CP+TW\ DP)/(CP+DP) \qquad 5\text{-}6$$

Substituting for TOR in equation 5-1 gives:

$$QPZ = \frac{2\pi CP \cdot DP}{CP+DP}(TS-TW) \qquad 5\text{-}7$$

which is the equation for the steady-state heat flowrate per length of pipe at the longitudinal coordinate z in terms of the water and soil surface temperatures considering the thermal resistances of the soil and the pipe.

Analyzing a small, finite element of pipe, dz, as in Figure 5-3 under steady-state conditions gives:

$$0 = SPH \cdot MFR \cdot TINP - SPH \cdot MFR \cdot (TINP+(dTW/dz) \cdot dz)+QPZdz \qquad 5\text{-}8$$

where

SPH = specific heat of water (J/Kg/C)

MFR = mass flow rate of water (Kg/s)

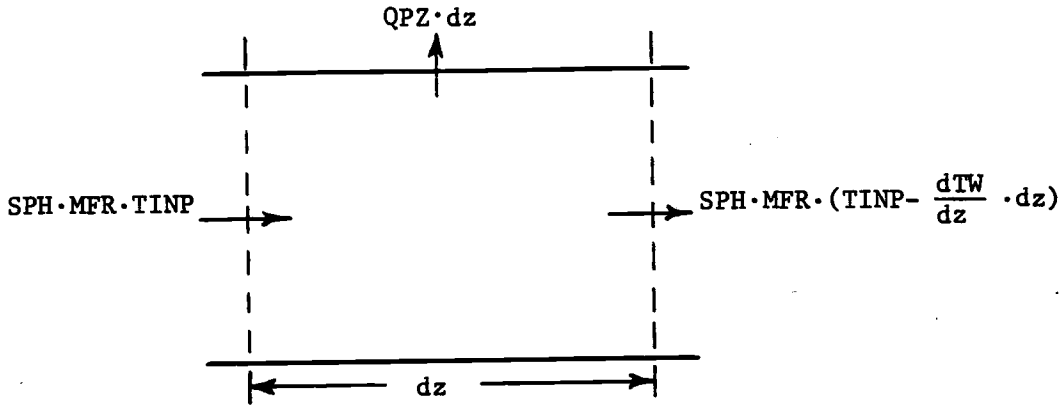

Figure 5-3. Small, finite element analysis of pipe.

TINP = incoming water temperature for the pipe (C)

TW = water temperature (C)

Substituting for QPZ and reducing gives:

$$dTW = \frac{2\pi CP \cdot DP(TW-TS)\ dz}{SPH \cdot MFR(CP+DP)} \qquad 5\text{-}9$$

The temperature in the pipe at a distance LC can be determined by integrating this equation from z=0 at water temperature TINP to z=LC at water temperature TOUTP, then solving for TOUTP. The integration gives:

$$\ln\left(\frac{TOUTP-TS}{TINP-TS}\right) = \frac{-2\pi CP \cdot DP \cdot LC}{SPH \cdot MFR(CP+DP)} \qquad 5\text{-}10$$

and

$$TOUTP = TS + (TINP-TS) \cdot \exp\left(\frac{-2\pi CP \cdot DP \cdot LC}{SPH \cdot MFR(CP+DP)}\right) \qquad 5\text{-}11$$

The overall rate of heat transfer from the pipe, QP, can be calculated from the change in the water temperature by:

$$QP = SPH \cdot MFR(TOUTP-TINP) \qquad (J/s) \qquad 5\text{-}12$$

The relationship for the overall heat transfer rate for buried pipes is derived from steady-state conditions with a constant soil surface temperature and a homogeneous soil. Considering these simplifying assumptions and the dynamics of soil heat transfer as presented in Chapter 3, an average daily value will be used for the soil surface temperature.

5.2 Heat Transfer From Above Ground Pipes

For heat transfer from pipes above ground the heat transfer per unit length of pipe is given by (Welty et al.,1976):

$$QPZ = 2\pi EP(TA-TW) \qquad 5\text{-}13$$

where

$$EP = \left(\frac{1}{HCONIP \cdot RI} + \frac{\ell n(TO/RI)}{KP} + \frac{1}{HCONOP \cdot RO}\right)^{-1} \qquad 5\text{-}14$$

HCONOP = convective heat transfer coefficient for the outside surface of the pipe ($J/m^2/s/C$) (Appendix D)

TA = air Temperature (C)

and all other variables are as defined in Section 5.1. Analyzing a small, finite element of pipe as in Figure 5-3 , Section 5.1, gives:

$$TOUTP = TA + (TINP-TA) \cdot \exp \frac{-2\pi EP \cdot LC}{SPH \cdot MFR} \qquad 5\text{-}15$$

and

$$QP = SPH \cdot MFR(TOUTP-TINP) \qquad (J/s) \qquad 5\text{-}16$$

5.3 Multi-Composite Pipes

For analysis of pipes composed of multiple layers of different materials, such as an insulated or coated pipe, the overall thermal conductive resistance, TCR, can be calculated for use in the equations for the heat transfer from buried and above ground pipes given in Sections 5.1 and 5.2. Given a multi-composite pipe as in Figure 5-4 the thermal conductive resistance is given by:

$$TCR = \frac{\ell n(R2/R1)}{K1} + \frac{\ell n(R3/R2)}{K2} + \frac{\ell n(R4/R3)}{K3} \qquad (m \cdot s \cdot C/J) \qquad 5\text{-}17$$

where

K(i) = the ith thermal Conductivity (J/m/s/C)

R(i) = the ith radius (m)

The thermal conductive resistance,TCR, replaces the expression for the single layer conductive resistance, ℓn(RO/RI)/KP, in the equations for the buried and above ground heat transfer analysis.

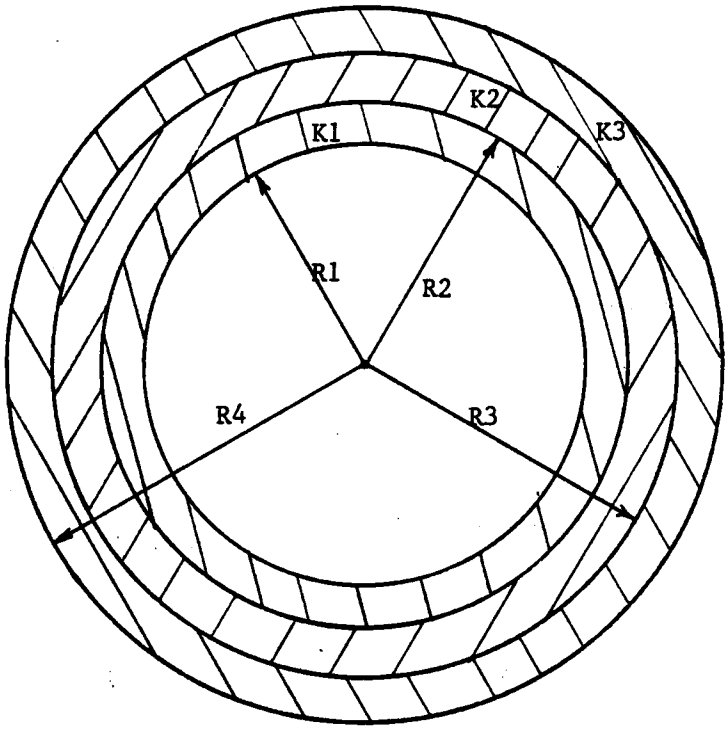

Figure 5-4. Multi-composite pipe.

CHAPTER 6

HEAT TRANSFER IN AERATION SYSTEMS

6.1 Introduction

The heat transfer which takes place between air and water during a forced aeration is the sum of the sensible and the latent heat exchanged. Heat may be transferred to or from an air bubble traveling through the water or a drop of water traveling through the air. The amount of heat exchanged is dependent on several variables that are highly specific to the aerator type, design and operating conditions. These variables include:

1) The volume and surface area of the air bubbles in contact with the water.
2) The volume and surface area of the water droplets in contact with the air.
3) The time of contact between the air and the water surfaces.
4) The velocity and the turbulent characteristics of the air and water which effects the thickness of the interface film layers.
5) The psychometric properties of the air.

These variables can be very difficult to measure and may have considerably different values even for the same type of aerator (Van De Donk,1981; Eckenfelder,1967; Thibodeaux,1979).

Considering the dependence of the aeration variables on the specific aeration system design and operating conditions, the lack of analytical or empirical relationships for determining these variables and the large number of different aeration types, this paper will focus on a more general approach to the heat transfer prediction. Two methods for approximating the heat transfer are

presented. One is for predicting the heat exchange between an air bubble and water and the other for the heat exchange between a water droplet and air. The use of these two theoretical methods requires estimates of the operating variables for the specific aerator being analyzed.

6.2 Heat Transfer Between Air Bubbles And Water

A volume of air traveling through water will undergo a change in both sensible and latent heat content due to several heat transfer processes. The total amount of heat exchanged can be determined from the change in the total heat content of the air. A change in heat content is given by the change in enthalpy. For an air-water vapor mixture the enthalpy is expressed by (Henderson,1976):

$$ENTH = SPHA \cdot TA + HMR(1000.\ XLAT + SPHV \cdot TA) \qquad 6\text{-}1$$

where

ENTH = enthalpy of air-vapor mixture (J/Kg-dry air)

TA = air temperature (C)

SPHA = specific heat of dry air (1006. J/Kg/C)

SPHV = specific heat of water vapor (1880. J/Kg/C)

HMR = humidity ratio of air (Kg-water/Kg-dry air)

XLAT = latent heat of vaporization (J/g)

The latent heat of vaporization is given by (Heinz et al.,1981):

$$XLAT = 2500.82 - 2.3576\ TW \qquad 6\text{-}2$$

where

TW = water temperature (C)

The humidity ratio is calculated from (Henderson,1976):

$$HMR = \frac{EA}{1.608(PA-EA)} \qquad 6\text{-}3$$

where

EA = vapor pressure at the air temperature TA (mb) (Section 2.5)

PA = atmospheric pressure (mb)

The rate of heat exchange between the air and water can be calculated from the mass rate of the air traveling through the water

and the initial and final values of the heat content (enthalpy) of the air. The relationship is:

$$HAER = MAIR(ENIN-ENOUT) \qquad 6\text{-}4$$

where

HAER = the overall heat exchange rate between the entrained air and the water (J/s)

MAIR = mass flowrate of dry air (Kg-dry air/s)

ENIN = enthalpy of the incoming air (J/Kg-dry air)

ENOUT = enthalpy of the outgoing air (J/Kg-dry air)

The mass flowrate of dry air, MAIR, can be determined from the flowrate or entrainment rate of air in conjunction with the ideal gas law and Dalton's law of partial pressures. Dalton's law states that the total pressure of a mixture of gases equals the sum of the partial pressures of the individual gases (MWPS,1981). Thus for an air vapor mixture:

$$PA = PDA+EA \qquad 6\text{-}5$$

where

PA = atmospheric pressure (mb)

PDA = partial pressure of dry air (mb)

EA = vapor pressure (mb) (Section 3.5)

From the ideal gas law the partial pressure of dry air can be expressed by:

$$PDA = MAIR \cdot GCA(TA+273.15) \cdot CVF/AFLOW \qquad 6\text{-}6$$

where

GCA = gas constant for air (287.0 J/Kg/K)

CVF = conversion factor (0.01 mb$\cdot$m^3/J)

AFLOW = volume flowrate of air-vapor mixture (m^3/s)

Substituting for PDA from the partial pressure relation (equation

6-5) and solving for the mass flowrate of dry air, MAIR, gives:

$$MAIR = \frac{AFLOW(PA-EA)}{GCA \cdot CVF(TA+273.15)} \qquad 6\text{-}7$$

Prediction of the heat exchange rate in entrained air or bubbling aeration systems requires estimates for several of the parameters used in equation 6-4. These estimates include the temperatures, vapor pressures and flowrates of the air entering and exiting the water. Conservative estimates for the entering and exiting air temperatures and vapor pressures (maximum heat transfer rate for cold weather conditions) are given by assuming the air entering the water is at the same temperature and vapor pressure as the ambient air and that the air leaving the water is at the same temperature as the water and has a saturated vapor pressure. The volume flowrate of air can be determined for diffused aeration aerators from the required oxygen addition and the operating specifications for the specific aerator (Metcalf and Eddy,1979). Van De Donk (1981) found that air entrainment by plunging jets is a complex phenomenon dependent on the jet parameters. However, the air entrainment rates were found to be on the same order of magnitude as the liquid flowrates for the jets. The air entrainment rate for surface aerators (paddle wheels, brushs, and fountains) is dependent on the specific aerator. Investigations showed that 50 percent of the total oxygen transferred by a surface aeration unit was transferred to the spray liquid and the remainder from the entrained air (Eckenfelder,1967). Methods for determining the entrainment rate for aerators has included photography and air entrapment techniques. Additional research is needed for estimating rates of air entrainment for surface aerators.

6.3 Heat Transfer Between Water Droplets and Air

A semi-empirical relationship for the change in temperature of a water droplet traveling through air developed by Best(1952) was shown to give satisfatory predictions in an experiment by Cline et al.(1969) on impact temperatures of heated irrigation water. The relationship considers the transfer of both sensible and latent heat and assumes there is no spatial temperature variation within the droplet. The relationship is:

$$\frac{dTWDR}{dt} = \frac{3\ VENT \cdot IV}{RDR^2 \cdot ROW2 \cdot SPH} \qquad 6\text{-}8$$

where IV is an intermediate value given by:

$$IV = \frac{KA(TA-TWDR)-XLAT \cdot DIFC \cdot 2(ESW-EA)}{GCW \cdot CVF2(TWDR+TA+546.3)} \qquad 6\text{-}9$$

and

t = time (s)

TWDR = water droplet temperature (C)

TA = air temperature (C)

ESW = saturation vapor pressure at the water droplet temperature TWDR (mb)

EA = vapor pressure at air temperature TA (mb)

RDR = water droplet radius (m)

GCW = gas constant for water (461.5 J/Kg/K)

CVF2 = conversion factor (10^{-5} mb$\cdot$m$^3\cdot$Kg/J/g)

XLAT = latent heat of vaporization (J/g)

DIFC = diffusion coefficient for water vapor in air (m/s)

ROW2 = density of water (Kg/m^3)

SPH = specific heat of water (J/Kg/C)

KA = thermal conductivity of air (J/m/s/C)

VENT = an empirical coefficient (referred to by Best as the ventilation coefficient)

Relationships are given in Section 2.5 for determining the values of ESW, EA and XLAT. The coefficient of diffusion for water vapor in air, DIFC, was observed to be 2.39×10^{-5} m^2/s at a temperature of 8 degrees centigrade by Guglielmo (Weast,1966) and Welty et al.(1976) give a value of 2.60×10^{-5} m^2/s for a temperature of 25 degrees centigrade at one atmosphere of pressure. The thermal conductivity of air, KA, is given by the following expression (Welty et al.,1976):

$$KA = .002544 + 7.9 \times 10^{-5}(TA+273.15) \quad (J/m/s/C) \qquad 6\text{-}10$$

The ventilation coefficient, VENT, is dependent on the Reynolds number, RE, and is given by (Best,1952):

$$VENT = 1. + 0.141RE^{0.6} \qquad 6\text{-}11$$

where

$$RE = 2 \cdot RDR \cdot VAIR/KVA \qquad 6\text{-}12$$

and

RDR = droplet radius (m)

VAIR = the water droplet velocity relative to the air (m/s)

KVA = kinematic viscosity of air ($1.4 \times 10^{-5} m^2/s$ at 7 C)

Equations 6-11 and 6-12 indicate that the ventilation coefficient is dependent on the velocity of the water droplet. This requires identification of the velocity throughout the droplet trajectory. Symon (1960) developed solutions for the equations of motion for a particle assuming air resistance as a frictional force that is proportional to the velocity. Given that the particle (droplet) starts from the origin at time T=0 the solutions are:

$$VX = VX0 \cdot \exp\left(\frac{-DRAG \cdot T}{MDR}\right) \qquad 6\text{-}13$$

and

$$VY = \left(\frac{VY0+MDR \cdot GRAV}{DRAG}\right) \cdot \exp\left(\frac{-DRAG \cdot T}{MDR}\right) - \frac{MDR \cdot GRAV}{DRAG} \qquad 6\text{-}14$$

where

VX = velocity component in the horizontal direction (m/s)

VY = velocity component in the vertical direction (m/s)

VX0 = initial horizontal velocity (m/s)

VY0 = initial vertical velocity (m/s)

MDR = mass of the water droplet (g)

GRAV = acceleration due to gravity (9.81 m/s^2)

DRAG = drag factor for air resistance ($g \cdot m/s^2$)

The drag factor, DRAG, is dependent on the size and shape of the water droplet as well as the viscosity of the air (Symon, 1960). It can be determined from experimental values of the terminal velocity (MDR·GRAV/DRAG). Experimental values for the terminal velocity as a function of droplet diameter are given in Figure 6-1 (Cline et al., 1969).

Cline et al.(1969) found that valid velocity components throughout the water droplet trajectory from the equations by Symon are obtained by using a small time increment of approximately one tenth of a second. This is also a suitable time increment for the determination of the cooling rate by the equation by Best (Cline et al., 1969). Thus for each new time increment of the analysis the new velocity is determined with the initial velocity equal to the preceding time increment final velocity and a new cooling rate is obtained. A new water droplet temperature is determined from the cooling rate for each step of the water droplet trajectory.

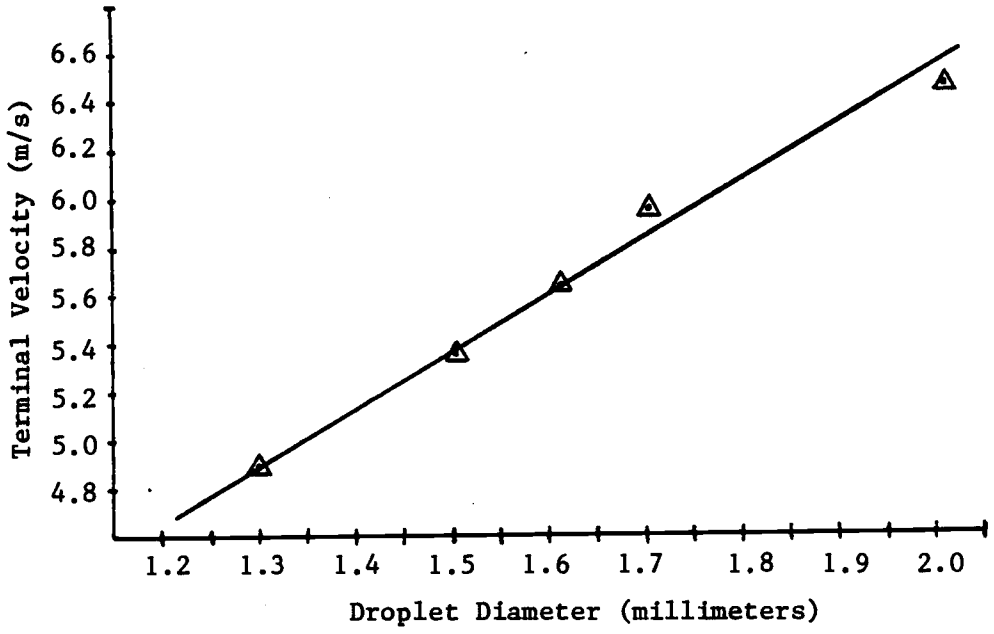

Figure 6-1. Terminal velocity versus droplet diameter.

A representative initial velocity, droplet diameter and total horizontal distance or time of travel must be identified for approximating the total change in temperature of the water droplet. In addition, the size distribution of water droplets represented by different parameters must also be determined. The heat transfer rate can be calculated for that portion of the flowrate of aerated water represented by the water droplet. The relationship is:

$$HDR = TCD \cdot MFDR \cdot SPH \qquad 6\text{-}15$$

where

HDR = heat exchange rate between water droplet and the air(J/s)

TCD = total change in temperature of the water droplet (C)

MFDR = mass flowrate of water displaced by aerator represented by the water droplet with TCD (Kg/s)

SPH = specific heat of water (J/Kg/C)

Droplet parameters and distributions may be difficult to identify for some aeration devices. Kohl (1974) found that the droplet size and initial velocity are a function of pressure and orifice size for agricultural sprinklers. Droplet sizes ranged between one and six millimeters for average size nozzles. Droplet velocities for sprinklers may be approximated from the orifice size and volume flow rate. Measurements taken by Boundurant et al.(1973) with photographs showed the droplet velocity for water surface agitators to be equal to half the impeller tip speed. Droplet diameters for the agitators ranged from 2.5 to 10 millimeters. Green (1952) found that droplet velocities and diameters can be measured with reasonable accuracy by means of photograghs. Given the wide range of droplet sizes reported and the difficulty in obtaining their

distribution, it appears that precise values of heat transfer rates may not be possible to predict without examining the specific aerator of interest to determine the droplet parameters. Hypothetical approximations of the heat exchange may be computed from the model based on estimated droplet parameters to make relative comparisons. Additional research is needed to determine the sensitivity of predicted heat transfer rates to changes in the droplet parameters.

CHAPTER 7

APPLICATION AND RESULTS

7.1 Assumptions of Application

A number of assumptions were made in development and presentation of the heat transfer relationships given in Chapters 2 through 6. Additional assumptions must be made in the application of these relationships. The following is a list and discussion of the assumptions made in the application of the comprehensive heat transfer model.

1) In the application of the model to plug flow reactors, the water is assumed to be completely mixed at a constant temperature equal to the arithmetic mean of the incoming and outgoing water temperatures. The net heat transfer rate is calculated from this average water temperature. A new outgoing temperature is then determined and the process is repeated in an iterative procedure until the new average temperature changes by less than 0.01 degrees centigrade. For the first iteration the water temperature is assumed to be equal to the incoming water temperature. An analytical solution by differential calculus is not possible due to the non-linear partial differential equation that results from the heat budget combination of the heat transfer relationships. Since the temperature change through the reactor is small due to the high heat capacity of the water, the constant temperature-complete mix assumption should not significantly affect the predicted heat transfer rate. However, in cases of extremely long reactors or large temperature changes through the reactor it may be necessary to divide the

reactor into analytical segments for solution by a finite difference method. In such a case the effects of dispersion may also need to be included. However calculations for a hypothetical 100 ft. segment of an open channel using a dispersion coefficient determined from a relationship given by Elder (1959) resulted in an insignificant amount of temperature dispersion. For complete mix reactors the water temperature used for calculating the heat transfer rate should be the outgoing water temperature determined by an iterative procedure.

2) The effects of vertical temperature stratification in the water are assumed to be negligable. For most aquaculture applications the water should be non-stratified due to the high rate of water replacement in raceway cultures and the requirement of aeration devices which cause vertical mixing in pond cultures. Most recycle systems of interest will involve a high density culture where movement of the organisms will also cause vertical mixing. However, vertical stratification may occur in deep water containments having slow flowrates or in systems where hot water is being added to a cooler body of water. Indepth discussions of methods for analyzing vertical stratification are presented by Jirka, et al. (1975) and Heinz, et al. (1981). Vertical temperature differences measured in the Oregon Aqua-Foods raceway near Springfield, Oregon were not large enough to measure (less than the 0.05 degree centigrade divisions on the thermometer).

3) It is assumed that the water surface temperature is equal to the bulk (completely mixed) water temperature. Ryan and Harleman (1973) note the formation of a thin (0.001 meter) cool surface skin

on many water surfaces. The water surface temperature at the Oregon Aqua-Foods Hatchery measured 0.1 degree centigrade below the bulk water temperature on a cold day and 0.1 degree above on a warm day. Such a small temperature difference would have an insignificant effect on the net heat transfer rate.

4) The use of the regional weather data values of dry bulb temperature and wet bulb temperature (or relative humidity) in place of the values at two meters above the water surface is assumed to have a negligible effect on the net heat transfer rate. This seems reasonable considering the relatively small bodies of water, and the moderate water temperatures involved in most recycle aquaculture facilities. This assumption also seems appropriate when considering the estimation purposes of the model and the limited historical data available for simulations.

5) The presence of heat sources and sinks around buried pipes is assumed to have a negligible effect on the heat transfer prediction. The theoretical relationship for buried pipes fails to account for such complexities. The application of the heat transfer relationships to pipes also assumes that the pipes are flowing full.

6) For heat transfer predictions using daily average climatic data the effect of solar radiation on walls ("sol-air" temperature concept) is neglected. For systems with large horizontal material surfaces exposed to sunlight or large vertical surfaces facing south, the solar effects on surface temperatures may need to be considered.

7) Analysis of diffused aeration heat transfer assumes that the air entering the water is at the same temperature and vapor pressure

as the ambient air and that air leaving the water is at the same temperature as the water with a saturated vapor pressure.

7.2 Materials and Methods for Predicted Versus Measured Rates of Heat Transfer

Comparisons of predicted and measured rates of heat transfer for a culture unit are based on data taken at the Oregon Aqua-Foods Fish Hatchery on March 28 and April 27, 1984 for a heated-water raceway containing coho salmon fingerlings. The hourly values of water temperature, dry bulb temperature, wet bulb temperature, barometric pressure, wind speed, and water flowrate were measured at the hatchery. Dimensions and materials were determined by measurements and by examination of the construction blue prints for the facility. Some secondary climatic data were obtained from local recording stations. These included hourly cloud cover readings, recorded at the National Weather Service Station at the Mahlon Sweet Airport in Eugene, Oregon; the hourly solar insolation values measured at the University of Oregon Solar Monitoring Laboratory in Eugene; and the average daily soil temperatures observed at the Oregon State University Hyslop Farm Experiment Station in Corvallis, Oregon. The climatic data and physical parameters used in the analysis are given in Appendices E and F.

In the application of the heat transfer model to the raceway, the detention time for the water was used as the time step of analysis. The climatic parameters for the end of the time step were obtained by interpolation of the hourly values. The average of the beginning and ending time step data was then used for predicting the heat transfer rates. The dry bulb and wet bulb air temperatures were measured over the water surface with an electrically aspirated psychrometer at approximately two meters above the water surface.

Total wind run values (average wind speeds) were obtained from an anemeter positioned at two meters above the water surface.

Measured rates of heat transfer were determined from the change in water temperatures at the beginning and end of the raceway along with the water flowrate and heat capacity. Some problems in obtaining useful data for measured heat transfer rates were encountered due to fluctuations in both the flowrate and the beginning water temperature during sampling. The values used in the following comparisons are from constant beginning water temperature and flowrate conditions. The water temperatures were recorded at the beginning and the end of the raceway with a 0. to 18. degree centigrade mercury thermometer having .05 degree divisions which allowed a .025 degree measurment sensitivity. The measurement for the begining water temperature was taken at the water pipe inlet to the raceway. The water temperature at the end of the raceway was measured at a depth of 0.2 meters and was identical to the temperature of the water leaving the raceway over the exit weir. Transverse (side to side) temperature readings were also observed which showed no measurable temperature difference across the raceway. The measurement accuracy of the thermometer was not considered in the analysis since the relative change in the water temperature was the value required for the measurement of heat transfer. The water flowrate was measured with an Annubar multiple opening pitot tube flow meter placed inside the incoming water pipe through a measurement port. The sensitivity of the meter was approximately 20 gallons per minute for the raceway being analyzed (750 gpm flowrate).

7.3 Results for Predicted Versus Measured Rates of Heat Transfer

The results of the predicted and measured rates of heat transfer for March 28 and for April 27 are given in Table 7-1. A range of values is given for the measured heat transfer rate based on the water temperature and flowrate measurements and the measurement sensitivities. It appears from these results that the model may be used successfully for approximating heat transfer rates from water containment structures, either in cases of heat loss or heat gain. Considering the limited amount of data obtained on the measured rates of heat transfer, it is difficult to draw substantial conclusions about the accuracy of the prediction model. Additional research using more sensitive instruments in a system which has better controls on the flowrate and the initial water temperature would be desirable to conclusively validate the model.

It should be noted from the results that the air-water interface was the primary location of predicted heat transfer for the raceway given the specific operating conditions and climatic data. For all four predictions, more than 95 percent of the net heat exchange was predicted to occur at the air-water interface. Heat exchange with the air-wall-water interface and heat exchange with the soil were almost insignificant. Subject to the limited amount of data analyzed it appears that net heat transfer approximations for water containment structures having large air-water interface areas may be made by analyzing the air-water interface, neglecting the soil and wall interfaces. This conclusion is examined further in the following applications of the model.

Table 7-1. Predicted versus measured values for Mar.28 and Apr.27.

Time (hr)	Water Temperatures (C)			Heat Transfer Rate (KJ/s)		
	In	Out	Out	Predicted	Measured	
(March 28)		(predicted)	(measured)		(min)	(max)
17.43	14.10	14.00	14.00	-19.10	-9.29	-29.46
18.43	14.10	13.89	13.90	-39.64	-27.88	-49.11
19.43	14.10	13.87	13.90	-43.08	-27.88	-49.11
(April 29)						
12.90	14.15	14.92	14.95	148.1	139.4	167.0

(Detention time = 1.52 hours on March 28)

(Detention time = 1.90 hours on April 29)

7.4 Daily Versus Three-Hour Heat Transfer Predictions

Daily and three-hour heat transfer predictions were calculated for a hypothetical raceway having operating and design characteristics similar to the Oregon Aqua-Foods Fish Hatchery raceway. The predictions were based on three-hour climatic observations for May 28 and December 23, 1983 recorded at the National Weather Service Station and the University of Oregon Solar Laboratory in Eugene, Oregon. The average climatic conditions for the three hour periods of analysis are determined from the climatic data. These average values are then used for predicting the three-hour rates of heat transfer over the 24-hour period. The average daily climatic conditions are then used to predict the 24-hour rates of heat transfer for comparison. Tables 7-2 and 7-3 give the results of the three-hour and daily predictions of heat transfer for the hot (May 28) and cold (December 23) days respectively. The climatic data for the two days of analysis and the physical parameters for the raceway are given in Appendices G and H.

The predicted total daily heat transfer for the cold day, using the average daily climatic data, was 75 percent of the total transfer predicted by the three-hour data. For the hot day, the prediction based on daily average data was 95 percent of the prediction based on three-hour data. Because of the rather large difference in the comparative results for the cold day data it appears that three-hour simulations would be required where precise values are of interest. For applications where relative values related to alternative operating or design parameters are of interest, the average daily data should give adequate predictions with less computer time

Table 7-2. Three-hour versus daily predicted heat transfer rates for May 28

Time (hr)	Heat Transfer Rate (KJ/s)	Heat Fluxes ($J/m^2/s$) Air-Water	Air-Wall-Water	Soil	Temperature Out (C)
3	-19.61	-81.58	.1955	2.331	13.90
6	-1.514	-9.626	2.538	2.372	13.99
9	120.3	475.9	3.772	2.084	14.63
12	230.2	914.2	2.461	1.861	15.20
15	178.1	706.5	3.556	1.968	14.93
18	45.76	178.9	2.752	2.238	14.24
21	8.202	29.19	1.493	2.326	14.04
24	-15.51	-65.23	.8411	2.314	13.92
Daily	133.1	527.2	1.535	2.056	14.69

(Total daily heat transfer by three-hour time step = 1.212×10^7 KJ)

(Total daily heat transfer by 24-hour time step = 1.150×10^7 KJ)

(Incoming water temperature = 14.00 C)

Table 7-3. Three-hour versus daily predicted heat transfer rates for December 23

Time (hr)	Heat Transfer Rate (KJ/s)	Heat Fluxes ($J/m^2/s$) Air-Water	Air-Wall-Water	Soil	Temperature Out (C)
3	-225.7	-890.8	-8.126	-5.410	12.83
6	-219.0	-864.3	-7.843	-5.427	12.86
9	-234.5	-926.3	0.1128	-5.441	12.78
12	-183.9	-724.0	-9.387	-5.522	13.04
15	-188.2	-741.5	-7.718	-5.516	13.02
18	-211.8	-835.5	-7.363	-5.507	12.90
21	-232.4	-917.6	-8.522	-5.457	12.79
24	-247.7	-978.3	-9.377	-5.412	12.71
Daily	-202.1	-797.0	-8.532	-5.461	12.95

(Total daily heat transfer by three-hour time step = -2.331×10^7 KJ)

(Total daily heat transfer by 24-hour time step = -1.746×10^7 KJ)

(Incoming water temperature = 14.00 C)

and cost.

The maximum rate of heat loss predicted from the three-hour data on December 23 was 248 kilowatts, which is 46 kilowatts greater than the average daily rate. For May 28, the maximum rate of heat gain was 230 kilowatts, which is 97 kilowatts greater than the average daily rate. It appears from the differences in rates of heat transfer predicted from the three-hour data versus the daily average data that for sizing estimates of the heating and chilling units, the maximum loading rates should be determined for extreme day conditions using three-hour climatic data.

The maximum drop in the water temperature on December 23, predicted from the three-hour data, was 1.29 degrees centigrade for a detention time of 1.43 hours. The temperature drop predicted by the average daily data was 1.05 degrees centigrade. The maximum water temperature rise predicted by the three-hour data on May 28 was 1.20 degrees centigrade for a 1.43 hour detention time. The average daily temperature rise was predicted at 0.69 degrees centigrade. Considering the relatively small changes in water temperature during an hour and a half detention time, under extreme weather conditions, the average values of temperature change appear to give satisfactory temperature estimates. However, where specific temperature extremes are important and the detention time through the system is substantial, the values predicted from three-hour observations of the climatic parameters may be significantly different.

The average daily heat flux rates at the air-water interface, air-wall-water interface, and soil-wall-water interface are listed in Tables 7-2 and 7-3 for the May 28 and December 23 simulations.

These values show that the major heat flux rate occurs at the air-water interface, and is greater than the other rates by more than two orders of magnitude. It appears from these values that for the specific system under analysis, adequate estimates of the net heat transfer rate for the water containment structure can be predicted entirely from the air-water heat flux. The large percentage of heat transfer at the air-water interface also shows the potential energy savings that may be realized by covering open water wherever possible. This point is further investigated in the application of the model to a hypothetical recycle system in the next section.

7.5 Sensitivity to Flowrate, Soil and Wall Thermal Conductivities, and the Water-Wall Thermal Convection Coefficient

The sensitivity of the net heat transfer rates to the flowrate, the soil and wall thermal conductivities, and the thermal convection coefficient between the water and wall was investigated for the hypothetical raceway using the average daily climatic data for May 28 and December 23 (Appendices G and H). The operating conditions and physical parameters for the analysis were identical to the conditions used for the 3 hour data versus 24 hour data calculations except for the specific sensitivity factor being investigated (flowrate, thermal conductivity, convection coefficient). The flowrate, FLOW, was increased to three times the original flowrate (from 0.046 m^3/s to 0.138 m^3/s). The thermal conductivity of the soil, KS, was doubled from 1.5 J/m/s/C (river rock and clay) to 3.0 J/m/s/C (wet quartz sand). The thermal conductivity of the wall, KW, was increased by two orders of magnitude from 1.2 J/m/s/C (concrete) to 120. J/m/s/C (aluminum) with a reduction in the wall width, WX, from 0.15 meters to 0.006 meters and a reduction in the material width of the base, BX, from 0.3 meters to 0.006 meters. The thermal convection coefficient between the water and wall,HCONW, was increased by 35 percent.

Table 7-4 gives the results of the average daily predicted heat transfer rates for the different changes in operating parameters. The average daily heat flux rates at the air-water, air-wall-water, and soil-wall-water interfaces are also listed in the table. These values show the insensitivity of the net heat transfer rates to the variables investigated. The changes in the net heat transfer rates

Table 7-4. Sensitivity analysis for flowrate, soil and wall thermal conductivities, and the water-wall thermal convection coefficient

Day	Parameter Changed	Heat Transfer Rate (KJ/s)	Heat Flux Rates ($J/m^2/s$) Air-Water	Air-Wall-Water	Soil
May 28	None	133.1	527.2	1.535	2.056
May 28	FLOW	133.8	529.7	1.585	2.278
May 28	KS	133.6	527.2	1.535	3.398
May 28	KW,WX,BX	133.3	527.2	1.573	2.550
May 28	HCONW	133.1	527.2	1.538	2.072
Dec.23	None	-202.1	-797.0	-8.532	-5.461
Dec.23	FLOW	-207.2	-816.7	-8.740	-5.860
Dec.23	KS	-203.4	-796.8	-8.531	-9.002
Dec.23	KW,WX,BX	-202.6	-796.9	-8.954	-6.801
Dec.23	HCONW	-202.2	-797.0	-8.561	-5.503

associated with these parameter changes were less than one percent, with the exception of the change in flowrate for December 23. The change in the net heat transfer rate due to the new flowrate on December 23 was less than three percent. It appears that where estimates or relative values of heat transfer rates are of interest, the accurate identification of these variables may not be critical. However, it should be recognized that these results are dependent on the specific climatic data and operating conditions being used in this particular analysis. The soil heat flux rate was increased by approximately 65 percent due to the change in soil thermal conductivity. This could cause a major change in the net heat exchange predictions in a system where the soil heat flux is a greater percentage of the net heat transfer rate.

7.6 Application to a Hypothetical Recycle System

Predictions of monthly heating reqirements were calculated for a seven month production schedule of coho salmon fingerlings in a hypothetical recycle system. Daily heat transfer rates are predicted for the culture unit, recycle water treatment units, and pipes based on the average daily climatic data and simulated operating conditions. The average daily recycle water temperature is then used with monthly average values of ambient make-up water to determine the heat required daily to maintain a specified water temperature. Heating costs are estimated from electric power rates in order to compare the relative economics of different operating stratagies.

The hypothetical system design is based on a 90 percent maximum recycle rate and is composed of a culture unit, sedimentation basin, biological filter, aeration basin, heat exchanger, and pipe network (Figure 7-1). The culture unit is a parallel set of two raceways similar in design to those operating at the Oregon Aqua-Foods Hatchery. Each raceway is 40 meters long by 5 meters wide with a 1.1 meter water depth. The average monthly flowrates (Appendix I) and the production capacity (7,500 Kg of fish per raceway) are from average operating conditions at the Oregon Aqua-Foods Hatchery for raising coho salmon fingerlings (25 to 35 grams) from eggs to release size over a seven month period from January to the end of July. The size of the sedimentation basin is equal to half the area of the culture unit with an equivalent depth. The biological filter design is based on a media requirement of one square foot of rock per gpm of water, four feet deep, with a six inch surface layer of

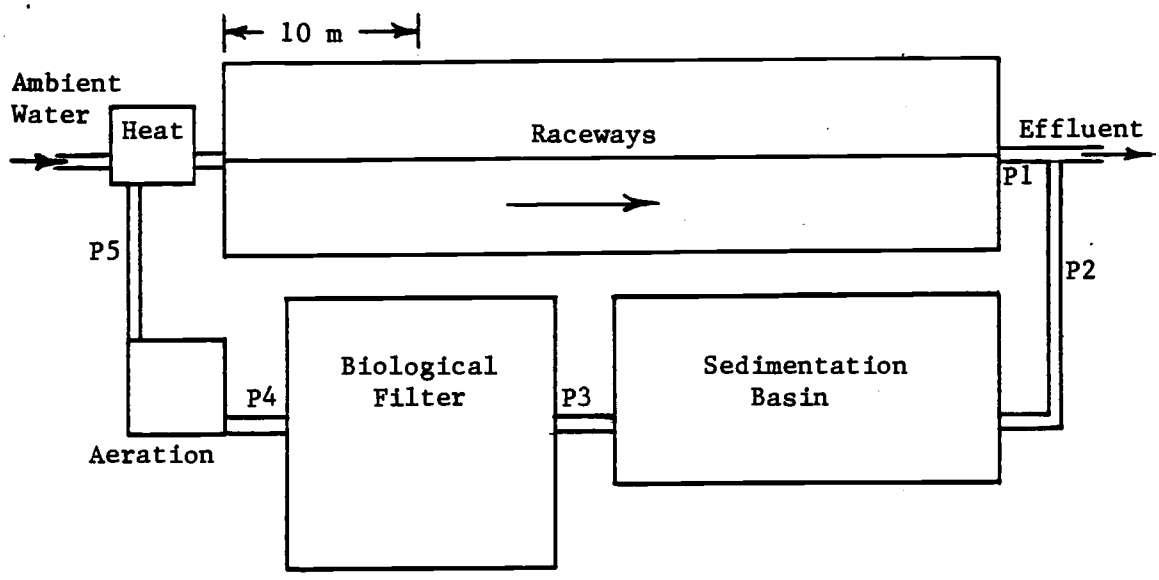

Figure 7-1. Hypothetical recycle salmon culture system.

crushed oyster shell (14 meters by 14 meters by 1.5 meters deep). The aeration basin (4 meters by 3 meters by 5 meters deep) is designed for nine-inch air diffusers based on the required air flowrate at the maximum oxygen demand and the diffuser specifications given by Aquatic Eco-Systems,Inc., Apopka, Florida. The required air flowrate in the aeration basin for each month during the period of the analysis is based on the average water flowrate for that month, an assumed oxygen deficit of 4 mg/liter, and a 10 percent oxygen transfer efficiency. The heat loss from the heat exchanger is accounted for by the efficiency rating of the unit. Appendix I lists the physical parameters for the system.

Ambient water temperature data from the Mckenzie River (a cold temperature Cascade Mountain river) and the Nestucca River (a moderate temperature coastal river) are used in the comparative applications of the model. Monthly average river temperatures are given in Table 7-5. The culture unit water temperature is held constant throughout each of the simulations at either 12 or 14 degrees centigrade. The climatic data used in the simulations are from average daily observations in 1983 at the Hyslop Farm Experiment Station at Corvallis and the National Weather Service Station at Salem. Appendix J gives the average monthly values of these data.

Heating requirements for maintaining the specified minimum water temperature in the culture unit were calculated. Days of excess water heat are assumed to require zero energy (no cooling). Under these circumstaces the recycle rate is decreased to lower the temperature. Average monthly values of water flowrates and ambient water temperatures are used in the analysis. For several of the

Table 7-5. Average monthly river temperatures

Month	McKenzie River Temperature (C)	Nestucca River Temperature (C)
January	4.70	7.99
February	5.18	6.57
March	6.19	8.10
April	7.03	9.12
May	8.33	11.19
June	10.14	12.00
July	11.32	15.80

simulations, the recycle rate was reduced during the final months of the production cycle when mass loading is at a peak level. The effect of covering the sedimentation basin and the biological filter to reduce energy losses at the air-water interface is investigated, as are the relative magnitudes of the pipe and aeration heat transfers.

Tables 7-6 and 7-7 give a summary of the heat transfer and economic simulations for 14 degree and 12 degree centigrade culture water temperatures respectively. The assumptions made concerning the economic calculations for these two water temperatures (discussed latter) are identical but it would be inappropriate to compare the resulting costs. This is due to the differences in the size, maturity and survival rates associated with the two seperate batches of fish. The fish reared in the 14 degree water would be larger at the end of the seven month rearing period and would be expected to have a greater return rate associated with their larger release size. In addition, the fish reared in the 12 degree water may not reach smolting stage by the required time of release and would therefore need to be held longer than the 14 degree water fish. The heating costs are given for relative comparisons of different operating conditions within the particular rearing temperature water.

Analysis of results for the extreme heat loss days for these simulations shows a maximum temperature drop through the system of 1.3 degrees centigrade during a system detention time of 6.5 hours (time required for the water to to travel through the raceway and water treatment units) with an initial water temperature of 14

Table 7-6. Comparison of heating and economic calculations for 14 C raceway water temperature.

River	Raceway Water Temp. (C)	Recycle Rate (percent)	Net Heat Requirement ($KW\text{-}hr \cdot 10^{-6}$)	Net Heat Cost (1000 $)	Heating Cost per lb Adult ($/lb)
McKenzie	14	90	1.08	45.0	.90
McKenzie	14	90+7mo.*	1.10	45.7	.91
McKenzie	14	90+3mo.**	.990	41.4	.83
McKenzie	14	(90,90,90,90, 70,50,20)***	2.86	119.0	2.40
McKenzie	14	none	11.4	467.0	9.30
Nestucca	14	90	.756	32.2	.64
Nestucca	14	(90,90,90,90, 90,70,50)	.886	37.1	.74
Nestucca	14	none	6.13	260.0	5.20

* = sedimentation and biological filter units covered for 7 months
** = sedimentation and biological filter units covered for 3 months (January, February, March)
*** = Recycle rate reduced for the final 3 months to 70, 50, and 20 respectively

Table 7-7. Comparison of heating and economic calculations for 12 C raceway water temperature.

River	Raceway Water Temp. (C)	Recycle Rate (percent)	Net Heat Requirement ($KW\text{-}hr \cdot 10^{-6}$)	Net Heat Cost (1000 $)	Heating Cost per lb Adult ($/lb)
McKenzie	12	90	.676	28.5	.45
McKenzie	12	90+7mo.*	.672	28.3	.57
McKenzie	12	90+3mo.**	.614	25.9	.52
McKenzie	12	(90,90,90,90, 70,50,20)***	1.33	55.3	1.10
McKenzie	12	(90,90,90,90, 90,70,50)	.841	34.9	.70
McKenzie	12	none	7.40	306.0	6.10
Nestucca	12	90	.448	19.5	.39
Nestucca	12	(90,90,90,90, 90,70,50)	.448	19.5	.39
Nestucca	12	none	2.17	99.7	1.99

* = sedimentation and biological filter units covered for 7 months
** = sedimentation and biological filter units covered for 3 months (January, February, March)
*** = Recycle rate reduced for the final 3 months to 70, 50, and 20 respectively

degrees centigrade. This relatively minor water temperature drop in the winter months coupled with a net heat gain from April through July results in a major heat energy savings through recycling. It is also observed that due to the minimal temperature loss within the recycle system, approximate estimates of the net heating requirements can be made based entirely on the required heat addition to the ambient make-up water. Net heat requirements for the seven month production schedule at 90 percent recycle rates estimated by this simplified model ranged from 80 percent of the complete model value (for moderate temperature coastal river water raised to 12 degrees centigrade) to 110 percent (for cold mountain river water raised to 14 degrees centigrade). Although these results may be sufficient for estimating the seven month heat requirements, it should be noted from the results that the energy estimates for specific months or days by this method do not adequately approximate the simulated values. Such estimates for critical intervals would be needed for determining the required design capacity of a heating, recycling system.

Observations of monthly heating requirements and average water temperatures for the simulations show a net heat gain through the recycle system for the months of April, May, June, and July which cause an overall net heat gain for the seven months of production. It thus appears that for the climatic conditions and culture water temperatures simulated in this analysis, the recycle system not only conserves heat, but collects heat to reduce the energy input required for the ambient water. This heat gain has important implications when considering conservation alternatives directed at

eliminating heat losses at air-water interfaces. The air-water interface is the major location of heat gain as well as heat loss. This is demonstrated by the simulation results for the McKenzie River water at a 90 percent recycle rate with the sediment basin and biological filter water surfaces covered with structural materials (Table 7-8). In these simulations the top of the sediment basin was assumed to be covered with a thin layer of expanded polystyrene and the biofilter was assumed covered with plywood. With these water treatment units covered for the entire production time, there was an estimated 33 percent decrease in the net heat gain through the recycle system for the 12 degree culture water and a three percent increase in the net heat gain (due to a decrease in the heat losses) for the 14 degree culture water. With the water surfaces covered only during the months of January, February, and March, there was an estimated 100 and 150 percent increase in the net heat gain through the recycle system for the 12 and 14 degree culture waters, respectively. This amounted to a 10 percent decrease in the net heating requirements for the system. An even higher percent reduction in the heating requirements would be expected from this energy conservation practice for warmer ambient water temperatures, such as the Nestucca River water, since the heat transfer within the recycle system is a higher percentage of the overall heat requirement of the production system.

The relative importance of the pipe and aeration heat losses was analyzed by comparing the net heat requirements for the system both with and without pipes and diffused air aeration. The proportion of the net heat transfer from the recycle system resulting from

Table 7-8. Comparison of heating requirements for covered sedimentation basin and biological filter water surfaces (McKenzie River, 90 percent recycle).

Conditions	Raceway Water Temp. (C)	Net Heat Requirement ($KW\text{-}hr \cdot 10^{-6}$)	Net Heat Gain in Recycle ($KW\text{-}hr \cdot 10^{-6}$)
no cover	12	.676	.064
no cover	14	1.08	.060
cover 7months	12	.672	.068
cover 7months	14	1.10	.040
cover 3months*	12	.614	.126
cover 3months	14	.990	.150

* = covered January, February, March

these factors is given in Table 7-9. The McKenzie River water with 90 percent recycling for 12 and 14 degree culture water was used for the analysis. The results demonstrate the relative insignificance of the pipe and aeration heat transfer for the particular conditions simulated. The calculated net heat loss from the pipes in the system was less than four percent of total heat transfer. The calculated net heat loss in the aeration process was less than two percent of the total for both the 12 and 14 degree simulations.

The total water heating costs and the heating cost per pound of harvested, adult salmon given in Tables 7-6 and 7-7 are based on the heating requirements for the water, the cost of electricity, an assumed water heater efficiency of 85 percent, a facility production rate of 500,000 coho salmon smolt per year (15,000 kilograms at 30 grams per smolt), and a one percent recapture rate of 10 pound adult coho salmon. The heating cost per smolt produced is equal to 10 percent of the cost per pound of harvested, adult salmon listed in the results. The electricity rates are from Pacific Power and Light Company rate schedule number 24 for domestic and farm service (June,1984). The assumed efficiency of the electric heater (85 percent) was suggested by Bolton, et al. (1935). This efficiency factor accounts for the transfer efficiency and the heat loss from the water heater. The smolt production rates are based on values recorded at the Oregon Aqua-Foods Hatchery and are consistent with the hypothetical system design.

Examination of simulated heating costs shows a wide range of values dependent on the culture water temperature, the ambient water temperature and the degree of recycling. The production of fish

Table 7-9. Heating requirements with and without pipes and aeration losses considered (McKenzie River, 90 percent recycle).

Factor	Raceway Water Temp. (C)	Net Heat Requirement with Factor ($KW\text{-}hr \cdot 10^{-6}$)	Net Heat Requirement Without Factor ($KW\text{-}hr \cdot 10^{-6}$)	Proportion of Net Heat Transfer from System (percent)
pipe	12	.6762	.6745	-2.6
pipe	14	1.081	1.079	-3.3
aeration	12	.6762	.6758	-0.6
aeration	14	1.081	1.081	-1.4

using the warmer ambient water of the Nestucca River, when compared with the cold McKenzie River water, reduced the operational heating costs by approximately 30 percent. The effect on the operational heating costs of reducing the 90 percent recycle rate during the final months of production varied from 167 percent to zero depending on the ambient water temperature and degree of reduction. Covering the sediment basin and biological filter water surfaces during the first three months of production reduced the heating costs by approximately 10 percent for the McKenzie River water.

The specific heating costs reported in Tables 7-6 and 7-7 are dependent on the simulation conditions for the heat transfer model and the assumptions made concerning the production rates of smolts and adult salmon. The high variability and degree of uncertainty associated with these values should be recognized. When specific costs are required for determining engineering economic present worth or rate of return values, it would seem advisable to run the model repeatedly with several different years of climatic data to determine the probability distributions of various outcomes. The costs are given here to demonstrate the value of the heat transfer model for relative ranking of alternative production strategies. It appears that in general, within the limitations, assumptions, and specific character of the results, release size coho fingerlings can be produced in a recycle system (in western Oregon climate and rivers) with an operational electric heating cost of less than ten cents per fish. The energy conservation practices that were evaluated by the heat transfer model could substantially reduce this production cost.

CHAPTER 8

CONCLUSION

A comprehensive heat transfer model has been developed for predicting heat transfer rates in an aquaculture facility. Heat transfer predictions for a salmon culture raceway at the Oregon Aqua-Foods Hatchery at Springfield, Oregon were compared to measured values. Three-hour predictions were compared to daily predictions for a hypothetical raceway. The application of the model was demonstrated in an analysis of heat transfer in a hypothetical recycle hatchery producing release-size coho salmon.

Comparisons of the predicted versus measured rates of heat transfer for a raceway showed that the model successfully approximated the net heat transfer rates within the sensitivity range of the measured values. The limited amount of data obtained on the measured rates of heat transfer make it difficult to conclusively demonstrate the accuracy of the model. Additional research is needed to test the accuracy of the model and to investigate the sensitivity of the heat transfer relationships to the climatic data and physical parameters. Comparison of predicted versus measured values of heat transfer rates in pipes and aeration processes would also be desirable.

A comparison of the predicted heat transfer rates based on three-hour and daily climatic parameters for a water containment structure resulted in the conclusion that three-hour data should be used when accurate values are of interest or when the predictions are being used for sizing temperature control units. For

applications where relative values related to alternative operation or design parameters are of interest, the average daily data should give adequate predictions with less computer time and cost.

The sensitivity analysis for the flowrate, the soil and wall thermal conductivities, and the water-wall thermal convection coefficient showed that for the specific raceway analyzed the accurate identification of these variables is not critical to the estimates of net heat transfer rates. For systems where the soil heat flux is a larger percentage of the net heat transfer rate the value used for the soil thermal conductivity would be of greater significance.

The air-water interfaces were found to be the primary locations of heat transfer in the analysis of both the raceway and the complete hypothetical facility with aeration and water treatment units. Heat exchange rates associated with all other locations (the air-wall-water interface, the soil, the pipes, and the aeration process) were relatively insignificant. The net heat transfer approximations for the specific systems investigated could be made by analyzing the air-water interface, neglecting all other factors. It appears that a very substantial reduction of heat losses from a system may be accomplished by covering open water surfaces during cold weather conditions.

The heat transfer simulations for a hypothetical recycle system showed that due to the minimal drop in the recycle water temperature during the winter months and the net heat gain during the months of April through July, there is a major heat energy savings realized by recycling. Also, due to the retention of heat in the recycled water, the net heating requirement for the total production time

could be roughly estimated by the heat requirement of the ambient make-up water. The climatic conditions and water temperatures used in this simulation resulted in a net heat gain from the environment over the seven months of production. There was therefore no substantial change in the simulated heating requirements when covers were placed on the sediment basin and biological filter for the entire time of production. However, when covers were in place only during the winter months (January through March) there was a 100 to 150 percent increase in the net heat gain for the system. It therefore appears that substantial energy savings can be accomplished by designing systems with removable water surface covers.

Simulations of production heating costs demonstrated the value of the heat transfer model for relative ranking of alternative production strategies. It should be recognized that these production heating costs are operating costs and do not include capital costs. Thus it would be wrong to compare operating costs alone unless all other costs were identical for the different production strategies. The operational heating costs for fish reared in 12 degree water were less than the costs for 14 degree water fish. However, this neglects the decrease in capital costs per fish produced in 14 degree water due to less facility production time that results from an increased growth rate (it's possible to raise two batches of 14 degree water fish in the production time required for one batch of 12 degree water fish). The operating costs were shown to be highly dependent on the culture water temperature, the ambient water temperature, and the degree of recycling. It was concluded that, within the limitations, assumptions, and specific character of

the results, release size coho salmon fingerlings can be produced within a recycle system with an operational, electric heating cost of less than ten cents per fish. In addition, energy conservation practices can substantially reduce this cost. The calculations of production heating costs demonstrated the value of the model for comparing the relative economics of alternative production strategies.

LIST OF REFERENCES

Anderson,E.R. 1954. Water Loss Investigations: Lake Hefner Studies. USGS Prof. Paper 269.

ASHRAE. 1981. American Society of Heating, Refrigerating and Air-Conditioning Engineers,Inc., Fundamentals Handbook. Atlanta,GA.

Best, A.C. 1952. The Evaporation of Rain Drops. Quarterly Journal Royal Meteorlogical Society, Vol 78,No.336, pp.200-225.

Bolton,D.J., P.C. Honey, N.S. Richardson. 1935. Electrical Water Heating. Chapman and Hall, L.T.D. London.

Boundurant, J.S., S. Lance, and H. Townsend. 1973. Unpublished chemical engineering senior project report, Dept. of Chemical Engineering, University of Arkansas, Fayetteville.

Bradey, D.K., W.L. Graves,Jr., J.C. Geyer. 1969. Surface Heat Exchange At Power Plant Cooling Lakes. Report No. 5, Edison Electric Institute, N.Y.

Campbell, G.S. 1977. An Introduction To Environmental Biophysics. Springe-Verlag, N.Y.

Carslaw, H.S. and Jaeger. 1959. Conduction of Heat In Solids. Oxford University Press, N.Y.

Cline, J.F., M.A. Wolf and F.P. Hungate. 1969. Evaporative Cooling of Heated Irrigation Water by Sprinkler Application. Journal of Water Resources Research, Vol.5,No.2, pp.401-406.

Colburn, A.P. 1933. Trans. American Institute Chemical Engineering, Vol.29, p.174.

Croft, R.D. and D.G. Lilley. 1977. Heat Transfer Calculations Using Finite Difference Equations. Applied Science Publishers LTD, London.

Douglas, M.J.M., and S.W. Churchill. 1956. Chemical Engrineering Progress Symposium Series,Vol.51, pp.17,57.

Eckenfelder,Jr., W.W. 1967. Manual of Treatment Processes; Oxygen Transfer and Aeration. Environmental Science Services Corp., Stanford, Conn.

Edinger, J.E., D.K. Brady and J.C. Geyer. 1974. Heat Exchange and Transport In The Environment. Report No. 14, Electric Power Research Institute, Palo Alto, Calif.

Edinger, J.E. and J.C. Geyer. 1965. Heat Exchange In The Environment. Edison Electric Institute, N.Y.

Elder, J.W. 1959. The Dispersion of Marked Fluid in Turbulent Shear Flow. Journal of Fluid Mechanics, Vol.5, pp.544-560.

Gates, D.M. 1965. Radiant Energy, Its Receipt and Disposal. Meteorol. Monogr. Vol.6,No.28, p.13.

Green, R.L. 1952. A Photographic Technique for Measuring the Sizes and Velocities of Water Drops From Irrigation Sprinklers. Agricultural Engineering, Vol.33,No.9, pp.563-586.

Gulliver, J.S. 1977. Analysis of Surface Heat Exchange and Longitudinal Dispersion in a Narrow Open Field Channel With Application To Water Temperature Prediction. M.S. Thesis, University of Minnesota, Dept. of Civil and Mineral Engineering, 187pp.

Heinz, G.S., J.S. Gulliver, M.G. Hahn, A.Y. Fu. 1981. Water Temperature Dynamics In Experimental Field Channels: Analysis and Modeling. St. Anthony Falls Hyd. Lab., University of Minnesota. pp.71-78.

Henderson, S.M., and R.L. Perry. 1976. Agricultural Process Engineering, Third Edition. AVI Publishing Co.,Inc. Westport, Conn.

Idso, S.B. and R.D. Jackson. 1969. Thermal Radiation From The Atmosphere. Journal of Geophysical Research, Vol.74,No.23, pp.5397-5403.

Ingersoll, L.R., O.J. Zobel and A.C. Ingersoll. 1948. Heat Conduction. McGraw-Hill Book Co., N.Y.

Jakob, Max. 1949. Heat Transfer, Volume I. John Wiley and Sons, Inc. N.Y.

Jirka, G.H., G. Abraham and D.R.F. Harleman. 1975. An Assessment Of Techniques For Hydrothermal Prediction. R.M. Parsons Laboratory for Water Resources and Hydrodynamics. Report No. 203. Massachusetts Institute of Technology.

Kenderick, J.H. and J.A. Havens. 1973. Heat Transfer Models For Subsurface, Water Pipe, Soil-Warming System. Journal Environmental Quality. Vol.2, pp.188-196.

Kohl, R.A. 1974. Drop Size Distribution From Medium-Sized Agricultural Sprinklers. Trans. ASAE. Vol.17,No.5, pp.690-693.

McQuiston, F.C. and J.D. Parker. 1982. Heating, Ventilating and Air Conditioning. John Wiley and Sons, Inc. N.Y.

Metcalf and Eddy, Inc. 1979. Wastewater Engineering. McGraw-Hill,N.Y.

Murray, F.W. 1967. On The Computation of Saturation Vapor Pressure. Journal of Applied Meterology, Vol.6,No.1, pp.203-204.

MWPS. 1981. Midwest Plan Service Structures and Environment Handbook. Iowa State University, Ames, Iowa.

MWPS. 1978. Midwest Plan Service Professional Design Supplement. Iowa State University, Ames, Iowa.

Paily, P.P., E.O. Macagno and J.F. Kennedy. 1974. Water-Regime Surface Heat Loss From Heated Streams. Institute of Hydraulic Research, Report No.155, University of Iowa.

Ryan, P.J. and D.R.F. Harleman. 1973. An Analytical and Experimental Study of Transient Cooling Pond Behavior. R.M. Parsons Laboratory For Water Resourses and Hydrodynamics, Report No.161, Massachusetts Institute of Technology. pp.28-95.

Sellers, W.D. 1965. Physical Climatology. University of Chicago Press, Chicago.

Shulyakovskiy, L.G. 1969. Formula For Computing Evaporation With Allowance For Temperature Of Free Water Surface. Soviet Hydrology Selected Papers, Issue No.6.

Symon, K.R. 1960. Mechanics. Addison-Wesley Publishing Co., Inc., Reading, Mass.

Tennessee Valley Authority. 1968. The Water Temperature Regime of Fully Mixed Streams. Water Resources Research Laboratory , T.V.A., Report No.15.

Thibodeaux, L.J. 1979. Chemodynamics: Environmental Movement of Chemicals In Air, Water, and Soil. John Wiley and Sons, N.Y.

U.S.G.S. Water-Data Report. 1982. Water Resources Data Oregon Water Year 1982, Vol.2.

U.S.G.S. Water-Data Report. 1981. Water Resources Data Oregon Water Year 1981, Vol.2.

Van De Donk, J.A.C. 1981. Water Aeration With Plunging Jets. Technische Hogeschool, Delft (Netherlands).

Van Wijk, W.R. 1963. Physics Of Plant Environment. North-Holland Publishing Co., Amsterdam.

Weast, R.C. and S.M. Selby. 1966. Handbook of Chemistry and Physics, 47th Edition. Chemical Rubber Co., Cleveland, Ohio.

Welty, J.R., C.E. Wicks and R.E. Wilson. 1976. Fundamentals of Momentum, Heat, and Mass Transfer. John Wiley and Sons, N.Y.

APPENDICES

APPENDIX A

List of Variables

AC = empirical constant for solar reflectivity

ACHANG = the average value of the cosine of the hour angle for the time step of analysis

AFLOW = volume flowrate of air-vapor mixture (m^3/s)

ALT = altitude in meters

AMP = amplitude of the sine function ($J/m^2/hr$)

AREA = cross-sectional area of channel (m^2)

AWAL = area of the air-wall-water interface (m^2)

AWAT = area of the air-water interface (m^2)

AZ = solar azimuth angle (the angle between south and the projection of the sun's rays on a horizontal plane) (radians)

BC = empirical constant for solar reflectivity

BOWEN = Bowen ratio

BX = material width of base (m)

CF = cloud cover fraction (0 to 1.)

CR = cloudiness ratio

CS = heat capacity of the soil ($J/m^3/C$)

CV = conversion factor ($0.11574\ cm^2 \cdot day/m^2/s$)

CVF = conversion factor ($0.01\ mb \cdot m^3/J$)

CVF2 = conversion factor ($10^{-5} mb \cdot m^3 \cdot Kg/J/g$)

D1 = declination of the sun (radians)

DAY = day of the year

DEP = depth pipe is buried, measured to the pipe centerline (m)

DEQ = equivalent diameter for channels (m)

DIFC = diffusion coefficient for water vapor in air (m/s)

DIA = diameter of the conduit (equivalent diameter for channels) (m)

DR = Total daily solar radiation on a horizontal surface(J/day)

DRAG = drag factor for air resistance ($g \cdot m/s^2$)

DRAD = the difference between the longwave radiation from the sky and surroundings, and from a black body at the air temperature ($J/m^2/s$)

DWC = depth of water in containment structure (m)

DX = depth of the containment structure below the surface (m)

EA = vapor pressure at air temperature TA (mb)

EA2 = vapor pressure at a height of 2 meters above the water surface (mb)

EAZ = vapor pressure at a height of z meters above the water surface (mb)

EMIS = clear sky emissivity

EMIT = emittance of the surface

ENIN = enthalpy of the incoming air (J/Kg-dry air)

ENOUT = enthalpy of the outgoing air (J/Kg-dry air)

ENTH = enthalpy of air-vapor mixture (J/Kg-dry air)

ES = saturated vapor pressure (mb)

ESA = saturated vapor pressure at air temperature TA (mb)

ESWB = saturated vapor pressure at air temperature TWB (mb)

ESW = saturated vapor pressure at the water temperature (mb)

FLOW = volume flow rate of water (m^3/s)

GCA = gas constant for air (287.0 J/Kg/K)

GCW = gas constant for water (461.5 J/Kg/K)

GND = normal direct radiation on a horizontal surface ($J/m^2/s$)

GRAV = acceleration due to gravity (9.81 m/s^2)

HA = longwave atmospheric radiation to water surface ($J/m^2/s$)

HAC = clear sky atmospheric radiation ($J/m^2/s$)

HAER = the overall heat exchange rate between the entrained air and the water (J/s)

HAI = incident longwave atmospheric radiation ($J/m^2/s$)

HANG = hour angle of the sun (radians)

HB = longwave back radiation from the water surface ($J/m^2/s$)

HC = conductive heat flux at the water surface ($J/m^2/s$)

HCONIP = convective heat transfer coefficient for the inside surface of the pipe ($J/m^2/s/C$)

HCONOP = convective heat transfer coefficient for the outside surface of the pipe ($J/m^2/s/C$)

HCONV = convective coefficient ($J/m^2/s/C$)

HCONVM = the modified convective coefficient ($J/m^2/s/C$)

HCONA = convective heat transfer coefficent between the air and the wall ($J/m^2/s/C$)

HCONW = convective heat transfer coefficient between the water and the wall ($J/m^2/s/C$)

HCR = coefficient of heat transfer by longwave radiation and convection at the outer surface ($J/m^2/s/C$)

HDR = heat exchange rate between the water droplets and the air (J/s)

HE = evaporative heat flux at the water surface ($J/m^2/s$)

HI = incident solar radiation on the water surface ($J/m^2/s$)

HIA = solar radiation incident to the outer atmosphere ($J/m^2/s$)

HIMAX = maximum clear sky solar radiation ($J/m^2/s$)

HIS = incident solar radiation on the containment surface ($J/m^2/s$)

HMR = humidity ratio of air (Kg-water/Kg-dry air)

HS = shortwave radiation (solar) on the water surface ($J/m^2/s$)

H1 = hour angle of the sun at time T minus the time step of analysis (radians)

H2 = hour angle of the sun at time T (radians)

INC = the angle of incidence for the surface (the angle between the sun's rays and the normal to the surface)

IR = incremental quantity of solar radiation (J)

IS = instantaneous solar radiation at time T ($J/m^2/hr$)

KC = coefficient dependent on cloud height

K(i) = thermal conductivity (J/m/s/C)

KA = thermal conductivity of air (J/m/s/C)

KP = thermal conductivity of the pipe material (J/m/s/C)

KS = thermal conductivity of the soil (J/m/s/C)

KVA = kinematic viscosity of air (m^2/s).

KW = thermal conductivity of the water containment material (J/m/s/C)

L = length of the containment structure (m)

LAT = geographic latitude (radians)

LC = length of the conduit (m)

MAIR = mass flowrate of dry air (Kg-dry air/s)

MC = atmospheric moisture content (cm)

MDR = mass of the water droplet (g)

MFDR = mass flowrate of water displaced by aerator represented by the water droplet having TCD (Kg/s)

MFR = mass flow rate of water (Kg/s)

MOL = molecular weight of water (18 g/g-mole)

MOPT = optical air mass

N = total daylight hours an day of analysis (hr)

PA = atmospheric pressure (mb)

PDA = partial pressure of dry air (mb)

PERIM = wetted perimeter of channel (m)

PR = Prandtl number (dimensionless)

PRATIO = ratio of air pressure at location altitude to sea level air pressure

QAWAT = heat transfer rate at the air-water interface (J/s)

QPZ = heat flowrate per linear unit length of pipe at longitudinal coordinate z (J/s/m)

QSIMP = net average daily heat transfer rate for simplified soil heat model (J/s)

QWAL = the overall heat transfer rate between air and water through the containment structure wall (J/s)

R(i) = radius (m)

RATIO = ratio of the actual to the mean distance from the sun to the earth

RDR = water droplet radius (m)

RE = Reynolds number (dimensionless)

REA = Reynolds number for air (dimensionless)

REFLEC = reflectivity of the water surface (0 to 1.)

RH = relative humidity (percent)

RI = inside radius of the pipe (m)

RO = outside radius of the pipe (m)

ROW = density of water (g/cm^3)

ROW2 = density of water (Kg/m^3)

SAB = solar absorptance of the surface

SB = Stefan-Boltzmann constant

SPH = specific heat of water (J/Kg/C)

SPHA = specific heat of dry air (1006. J/Kg/C)

SPHV = specific heat of water vapor (1880. J/Kg/C)

SRA = total daily solar radiation at the top of the atmosphere ($J/m^2/day$)

STEP = time step of analysis (s)

SUN = sun's altitude angle (radians)

t = time (s)

T = time of day (hr)

$T_{i,1}$ = soil temperature at the ith node at time T (C)

$T_{i,2}$ = soil temperature at the ith node at time T plus the time step of analysis (C)

T0 = steady-state soil temperature for the node (C)

T1 = steady-state soil temperature for the node (C)

T2 = steady-state soil temperature for the node (C)

TA = air temperature (C)

TA2 = air temperature at a height of 2 meters above the water surface (C)

TB = average daily soil temperature at a depth of DX plus two meters (C)

TCOEF = the overall heat transfer coefficient for the wall ($J/m^2/s/C$)

TCD = total change in temperature of the water droplet (C)

TCR = thermal conductive resistance for multi-composite pipes ($m \cdot s \cdot C/J$)

TD = dewpoint temperature (C)

TEM = temperature of the air-vapor mixture (C)

TILT = angle of tilt for the surface (radians)

TINP = incoming water temperature for pipe (C)

TOR = temperature of the pipe surface at the outside radius of the pipe, RO, at longitudinal coordinate z (C)

TOUTP = outgoing water temperature for pipe (C)

TRISE = time of sunrise (hr)

TS = temperature of the soil surface (C)

TSOL = sol-air temperature (C)

TSO = average daily soil temperature at a depth of one half DX (C)

TS1 = average daily soil temperature at a depth of DX plus one meter (C)

TSET = time of sunset (hr)

TSS = average daily soil surface temperature (C)

TSUR = surface temperature (C)

TW = water temperature (C)

TWB = wet bulb temperature (C)

TWDR = water droplet temperature (C)

V = volume of water within containment structure (m^3)

VAIR = the water droplet velocity relative to the air (m/s)

VEL = velocity of water (m/s)

VENT = an empirical (ventilation) coefficient

VIRT = virtual temperature difference between air at the water surface and at 2 meters (C)

VISC = kinematic viscosity of water (1.37×10^{-6} m^2/s at 10 C)

VX = velocity component in the horizontal direction (m/s)

VXO = initial horizontal velocity (m/s)

VY = velocity component in the vertical direction (m/s)

VYO = initial vertical velocity (m/s)

WFUNC2 = wind function for 2 meters above the water (cm/day/mb)

WFUNCZ = wind function for height z above the water (cm/day/mb)

WIND = wind speed (m/s)

WR = inside width of containment structure (m)

WSA = wall solar azimuth angle (radians)

WX = material width of the containment walls (m)

WZ = wall azimuth angle (radians)

X = soil cell width for finite difference grid (m)

XLAT = Latent heat of vaporization (J/g)

APPENDIX B

Modeling Solar Radiation As A Sine Function

Average solar radiation values for time increments of less than one day can be approximated from the total daily values by modeling the radiation as a sine function. Figure B-1 represents solar radiaton versus time of day as a sine function relationship. Assuming the total number of daylight hours is equal to half the period of the sine function gives the following equations.

For $TRISE \leq T \leq TSET$:

$$IS = AMP \cdot \sin \frac{\pi}{N}(T-TRISE) \qquad B-1$$

For $T \leq TRISE$ or $T \geq TSET$:

$$IS = 0 \qquad B-2$$

where

IS = instantaneous solar radiation at time T ($J/m^2/hr$)

AMP = amplitude of the sine function ($J/m^2/hr$)

N = total daylight hours (hr)

T = time of day (hr)

TRISE = time of sunrise (hr)

TSET = time of sunset (hr)

The value of the sine function amplitude, AMP, for a specific day can be determined from the total daily solar radiation, DR, which is equal to the area under the curve of the solar sine function. It can be shown by integrating the area under the sine function from time TRISE to TSET and setting it equal to DR that the amplitude is:

$$AMP = \frac{DR \cdot \pi}{2N} \qquad B-3$$

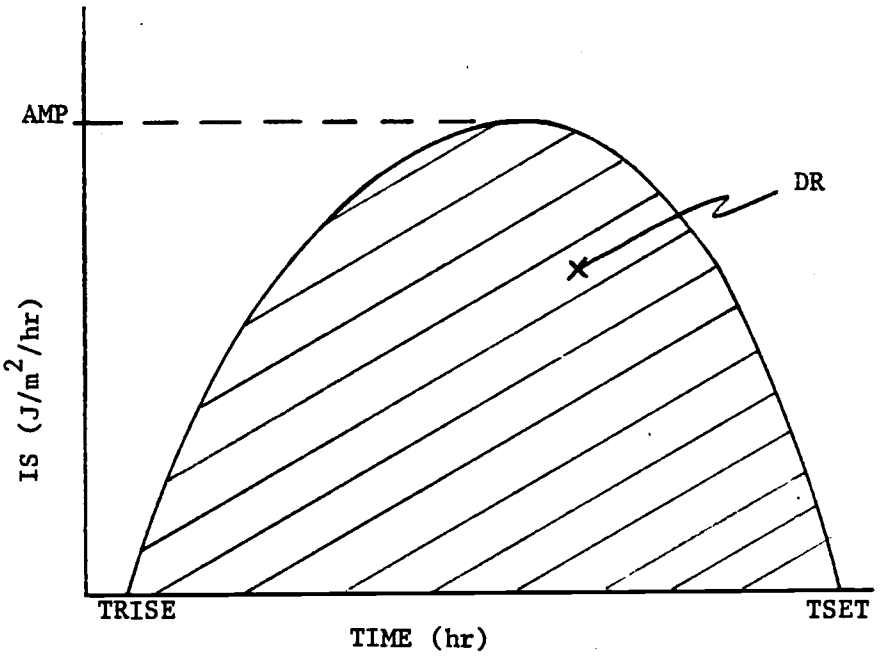

Figure B-1. Solar radiation versus time.

Substituting AMP into the equation for the instantaneous solar radiation, IS, and integrating over the time increment of interest, T1 to T2, gives the incremental quantity of solar radiation, IR :

$$IR = \frac{DR}{2} \cos \frac{\pi}{N}(T1-TRISE) - \cos \frac{\pi}{N}(T2-TRISE) \quad (J/m^2) \qquad B-4$$

Dividing IR by the time increment, T2 minus T1, gives the average rate of solar radiation for the time step of analysis.

APPENDIX C

Solar Obstructions

Objects such as trees, buildings or mountains may obstruct solar radiation at certain times of the year or day. The angle these objects make with the horizon (altitude angle) and the angle east or west of true south (azimuth angle) can be identified in the field. When the solar altitude and azimuth angles are within these obstruction angles, the solar radiation is zero. The solar altitude angle, SUN, is identified in section 2.2 and the solar azimuth angle, AZ, is given by (McQuiston and Parker,1982):

$$\sin(AZ) = \cos(D1)\sin(HANG)\cos(SUN) \qquad C\text{-}1$$

where

D1 = declination of the sun (Section 2.2)

HANG = hour angle of the sun (Section 2.2)

APPENDIX D

Convection Coefficients

D.1 Convection Coefficients for Water

The convective coefficient for the energy exchange between a conduit surface and a fluid in turbulent, internal flow is approximated from correlations of experimental data as suggested by dimensional analysis (Welty et al.,1976). The convection coefficient for water can be represented by the Colburn (1933) equation:

$$HCONV = 23RE^{-0.2} \cdot PR^{(-2/3)} \cdot SPH \cdot VEL \cdot ROW \qquad D\text{-}1$$

where

HCONV = convective coefficient ($J/m^2/s/C$)

RE = Reynolds number (dimensionless)

$$= DIA \cdot VEL/VISC \qquad D\text{-}2$$

PR = Prandtl number (dimensionless)

= approximatly 10. at 10. deg. centigrade for water

SPH = specific heat of water (J/Kg/C)

VEL = velocity of water (m/s)

ROW = density of water (g/cm^3)

and

DIA = diameter of the conduit (equivalent diameter, DEQ, for channels) (m)

VISC = kinematic viscosity of water (1.37×10^{-6} m^2/s at 10 C)

DEQ = equivalent diameter for channels (m)

$$= 4 \cdot AREA/PERIM$$

AREA = cross-sectional area of channel (m^2)

PERIM = wetted perimeter of channel (m)

The requirements for application of the Colburn equation are:

(1) RE and PR are evaluated at the film temperature and SPH and ROW are evaluated at the bulk temperature

(2) RE, PR and LC/DIA should have values within the following limits:

$$RE > 10^4 \qquad 0.7 \leqslant PR \leqslant 160. \qquad LC/DIA > 60.$$

where

LC = length of the conduit (m)

DIA = diameter of the conduit (equivalent diameter for channels) (m)

The following equations may be used to modify the convective heat transfer coefficient for passages in which LC/DIA is less than 60.

For $2. \leqslant LC/DIA \leqslant 20.$:

$$HCONVM = HCONV \cdot (1. + (DIA/LC)^{0.7}) \qquad \text{D-4}$$

For $20. \leqslant LC/DIA \leqslant 60.$:

$$HCONVM = HCONV \cdot (1. + 6 \cdot DIA/LC) \qquad \text{D-5}$$

where

HCONVM = The modified convective coefficient ($J/m^2/s/C$)

D.2 Convection Coefficients for Air

The forced-air convective heat transfer coefficient for air at the outside surface of a pipe can be determined from correlations of data for the flow of air normal to a single cylinder as given in Welty et al.(1976). For cases where the Reynolds number is greater than 500 they recommend an empirical relationship by Douglas and Churchill(1956)given by:

$$HCONOP = \frac{KA}{LC}(0.46REA^{1/2} + 0.00128REA) \qquad D\text{-}6$$

And for Reynolds numbers less than 500 they give the following equation by Hsu(1963):

$$HCONOP = \frac{KA}{LC}(0.43 + 0.48\ REA^{1/2}) \qquad D\text{-}7$$

where

HCONOP = convective heat transfer coefficient for the outside surface of the pipe ($J/m^2/s/C$)

KA = thermal conductivity of air ($2.5x10^{-2}$ J/m/s/C at 10 C)

REA = Reynolds number for air

$$= DIA \cdot WIND/KVA \qquad D\text{-}8$$

and

WIND = wind speed (m/s)

KVA = kinematic viscosity of air ($1.42x10^{-5}$ m^2/s at 10 C)

For vertical plane surfaces, the forced-air convection relationships given by the Professional Design Supplement to the MWPS Structures and Environment Handbook (1978) are:

$$HCONA = 7.345 \times 10^{-2} \cdot WIND^{0.8} \qquad D\text{-}9$$

when WIND is between 5. and 30. m/s and

$$HCONA = 5.622 \times 10^{-2} + 3.91 \times 10^{-2} \cdot WIND \qquad D\text{-}10$$

when WIND is less than 5. m/s.

APPENDIX E

Climatic Data for Oregon Aqua-Foods Raceway

Time (hr)	Dry Bulb Air Temp. (C)	Wet Bulb Air Temp. (C)	Barometric Pressure (mb)	Total Wind (mi)	Cloud Cover (tenths)	Solar Insolation (KJ/m^2)
Mar.28						
16	10.56	7.22	1010		10	
				1.7		393
17	10.00	6.11	1011		10	
				2.4		81
18	7.50	6.39	1011		10	
				2.7		14
19	6.94	6.11	1012		10	
				1.7		0
20	6.67	5.83	1012		10	
Apr.27						
11	12.78	9.44	1023		0	
				8.9		2986
12	15.00	10.00	1023		1	
				5.1		2858
13	16.11	10.00	1023		1	

Day	TRISE*	TSET	TSS	TS0	TS1	TB
Mar.28	5.50	18.60	10.0	8.06	11.1	11.1
Apr.27	5.17	19.18	14.2	9.70	11.9	11.9

*
TRISE = time of sunrise (hr)
TSET = time of sunset (hr)
TSS = average daily soil surface temperature (C)
TS0 = average daily soil temperature at half the buried depth of the raceway (C)
TS1 = average daily soil temperature at the buried depth of the raceway plus one meter (C)
TB = average daily soil temperature at the buried depth of the raceway plus two meters (C)

APPENDIX F

Physical Parameters for Oregon Aqua-Foods Raceway

Volume flowrate of water (FLOW) = 0.0457 m^3/s

Latitude (LAT) = 0.77 radians

Altitude (ALT) = 146. meters

Base material width (BX) = 0.305 meters

Width of walls (WX) = 0.152 meters

Inside width of raceway (WR) = 6.095 meters

Length of the raceway (L) = 44.2 meters

Depth of raceway below the surface (DX) = 1.168 meters

Depth of water in the raceway (DWC) = 0.876 meters (March 28)

Depth of water in the raceway (DWC) = 1.16 meters (April 27)

Area of the air-wall-water interface (AWAL) = 4.16 m^2 (March 28)

Area of the air-wall-water interface (AWAL) = 14.7 m^2 (April 27)

Area of the air-water interface (AWAT) = 250.8 m^2

Thermal conductivity of raceway walls (KW) = 1.2 J/m/s/C (concrete)

Thermal conductivity of soil(KS) = 1.5 J/m/s/C(river rock and clay)

APPENDIX G

Climatic Data for Hypothetical Raceway

G.1 Three-Hour Average Climatic Data

Time Step (hr)	Dry Bulb Air Temp. (C)	Wet Bulb Air Temp. (C)	Barometric Pressure (in-Hg)	Wind Speed (mi/hr)	Cloud Cover (tenths)	Solar Insolation (KJ/m^2)
May 28						
1-4	15.3	14.7	29.42	5.8	3	0
4-7	16.7	15.6	29.45	2.3	1	1131
7-10	22.5	18.6	29.46	3.5	0	6201
10-13	28.9	21.1	29.43	6.9	5	9544
13-16	31.4	22.5	29.38	9.2	10	6224
16-19	27.2	20.8	29.36	9.2	10	1046
19-21	20.3	16.4	29.39	10.9	10	19
21-1	16.4	13.3	29.44	17.3	9	0
Dec.23						
1-4	-11.4	-12.5	29.93	15.5	0	0
4-7	-11.9	-12.8	29.91	14.4	0	0
7-10	-11.1	-11.9	29.90	19.0	1	889
10-13	-7.78	-9.44	29.84	23.0	1	3544
13-16	-5.83	-7.78	29.75	20.1	2.5	1847
16-19	-7.22	-8.61	29.70	17.3	2.5	37
19-21	-8.89	-10.0	29.69	19.0	4.5	0
21-1	-9.17	-10.6	29.66	21.3	8.5	0

G.2 Average Daily Climatic Data

DAY	TRISE*	TSET	TSS	TSO	TS1	TB
May 28	4.56	19.8	23.6	14.4	15.3	15.3
Dec.23	7.78	16.6	-8.90	4.70	11.1	11.1

*

TRISE = time of sunrise (hr)
TSET = time of sunset (hr)
TSS = average daily soil surface temperature (C)
TSO = average daily soil temperature at half the buried depth of the raceway (C)
TS1 = average daily soil temperature at the buried depth of the raceway plus one meter (C)
TB = average daily soil temperature at the buried depth of the raceway plus two meters (C)

APPENDIX H

Physical Parameters for Hypothetical Raceway

Volume flowrate of water (FLOW) = 0.046 m^3/s

Latitude (LAT) = 0.769 radians

Altitude (ALT) = 109. meters

Base material width (BX) = 0.3 meters

Width of walls (WX) = 0.15 meters

Inside width of raceway (WR) = 6.1 meters

Length of the raceway (L) = 44. meters

Depth of raceway below the surface (DX) = 1.17 meters

Depth of water in the raceway (DWC) = 0.88 meters

Area of the air-wall-water interface (AWAL) = 8.4 m^2

Area of the air-water interface (AWAT) = 251. m^2

Thermal conductivity of raceway walls (KW) = 1.2 J/m/s/C (concrete)

Thermal conductivity of soil(KS) = 1.5 J/m/s/C(river rock and clay)

APPENDIX I

Physical Parameters for Hypothetical Recycle System

AFLOW = volume flowrate of air-vapor mixture (m^3/s)
ALT = altitude in meters
AWAL = area of the air-wall-water interface (m)
AWAT = area of the air-water interface (m^2)
BX = material width of base (m)
DEP = depth pipe is buried (m)
DWC = depth of water in containment structure (m)
DX = depth of the containment structure below the surface (m)
FLOW = volume flow rate of water (m^3/s)
KS = thermal conductivity of the soil (J/m/s/C)
KW = thermal conductivity of the water containment material (J/m/s/C)
L = length of the containment structure (m)
LC = length of pipe (m)
LAT = geographic latitude (radians)
RI = inside radius of pipe (m)
RO = outside radius of pipe (m)
TCR = thermal conductive resistance for multi-composite pipe (m·s·C/J)
WR = inside width of containment structure (m)
WX = material width of the containment walls (m)

Facility

LAT = 0.777
ALT = 30.
KS = 1.6 (wet clay soil)
KW = 1.2 (concrete)

Raceway

FLOW = 0.038 (Jan.)
FLOW = 0.063 (Feb.)
FLOW = 0.088 (Mar.)
FLOW = 0.101 (Apr.)
FLOW = 0.113 (May)
FLOW = 0.120 (June)
FLOW = 0.126 (July)
BX = 0.25
WX = 0.15
WR = 10.0
L = 40.
DX = 1.0
DWC = 1.1
AWAL = 35.
AWAT = 400.

Sedimentation Basin

BX = 0.25
WX = 0.15
WR = 10.
L = 20.
DX = 1.
DWC = 1.1
AWAL = 21.
AWAT = 200.

Biological Filter

BX = 0.25
WX = 0.25
WR = 14.
L = 14.
DX = 0
DWC = 1.5
AWAL = 84.
AWAT = 196.

Aeration Basin

BX = 0.25
WX = 0.25
WR = 5.
L = 5.
DX = 0
DWC = 3.
AWAL = 60.
AWAT = 25.
AFLOW = 0.2154 times the water flowrate through the basin

Pipes (see Figure 7-1)

	P1	P2	P3	P4	P5
RI =	0.3	0.255	0.255	0.255	0.255
RO =	0.35	0.283	0.238	0.238	0.238
LC =	3.0	17.	5.0	4.0	8.0
DEP =	1.0	1.	0.	0.	0.5
TCR* =	0.154	0.084	0.084	0.084	0.084

* concrete coated steel pipe

APPENDIX J

Average Monthly Values of the Daily Climatic Data for the Hypothetical Recycle System

Month	TA*	RH	PA	WIND	CF	HI	TSS	TSO	TS1
Jan.	5.69	85.2	1007	3.14	0.90	39.8	5.71	4.03	8.85
Feb.	7.61	82.0	1002	3.45	0.82	65.7	7.85	4.86	9.01
Mar.	9.69	80.8	1001	3.32	0.85	89.2	10.1	6.90	10.3
Apr.	10.1	72.5	1009	2.65	0.64	177.	11.0	8.06	11.1
May	13.9	72.5	1011	2.71	0.55	260.	14.7	11.7	13.4
June	15.2	71.7	1010	3.03	0.71	231.	16.3	14.7	16.1
July	17.2	73.3	1010	2.80	0.65	230.	18.3	15.0	17.1

*

TA = air temperature (C)
RH = relative humidity (percent)
PA = atmospheric pressure (mb)
WIND = wind speed (m/s)
CF = cloud cover fraction (0 to .1)
HI = incident solar radiation on the water surface ($J/m^2/s$)
TSS = soil surface temperature (C)
TSO = soil temperature at one half the buried depth of the raceway
TS1 = soil temperature at the buried depth of the raceway plus one meter